

POLITECNICO DI TORINO



Master's Degree in Biomedical Engineering

Design of a stretchable, conductive  
silicone-based biomaterial  
for vocal fold models

Supervisors:

Prof. Gianluca Ciardelli

Prof. Valeria Chiono

Dr. Irene Carmagnola

Dr. Giulia Giuntoli

Candidate:

Michele Mosca

A.Y. 2020/2021

# Summary

<b>Abstract</b> .....	<b>1</b>
<b>1 Introduction</b> .....	<b>3</b>
<b>1.1 Anatomy of the larynx</b> .....	<b>3</b>
1.1.1 Cartilages .....	3
1.1.2 Muscles .....	4
1.1.3 Vocal Folds .....	6
<b>1.2 Vocal folds models</b> .....	<b>8</b>
<b>1.3 Conductive Polymers</b> .....	<b>10</b>
1.3.1 Intrinsically Conductive Polymers .....	11
1.3.2 Extrinsically Conductive Polymers .....	14
1.3.3 Ionic Conductive Hydrogels .....	16
<b>1.4 Silicones</b> .....	<b>16</b>
1.4.1 Silicone Elastomers .....	17
1.4.2 Biomedical Silicones .....	18
<b>1.5 Aim of the Work</b> .....	<b>20</b>
<b>2 Materials and Methods</b> .....	<b>22</b>
<b>2.1 Materials</b> .....	<b>22</b>
2.1.1 PEDOT:PSS .....	22
2.1.2 Surfactant and Dopant .....	24
2.1.3 Silicone Elastomers .....	25
<b>2.2 Blends Preparation</b> .....	<b>25</b>
<b>2.3 Mechanical Tests</b> .....	<b>27</b>
2.3.1 Uniaxial Tensile Test at Break .....	27
2.3.2 Uniaxial Cyclic Tensile Test .....	29
<b>2.4 Water Contact Angles Measurements</b> .....	<b>30</b>
<b>2.5 ATR Fourier-transform Infrared Spectroscopy</b> .....	<b>31</b>
<b>2.6 Indirect Cytotoxicity Test</b> .....	<b>32</b>

2.7	Statistical Analysis.....	33
<b>3</b>	<b>Results and Discussion.....</b>	<b>34</b>
3.1	Uniaxial tensile test at break .....	36
3.2	Uniaxial cyclic tensile test .....	40
3.3	ATR-FTIR analysis .....	44
3.4	WCA measurements.....	46
3.5	Indirect cytotoxicity test.....	48
<b>4</b>	<b>Conclusions .....</b>	<b>52</b>
<b>5</b>	<b>Bibliography.....</b>	<b>54</b>

# Abstract

Soft Robotics is based on soft and stretchable organic structures that imitates natural movements and finds widespread use in many biomedical applications: diagnosis, drug delivery, assistive and wearable devices, surgical tools, prostheses or artificial organs. The use of transducers such as sensors and actuators require that the materials used should also possess adequate electrical conductivity.

This thesis originates from the collaboration between Politecnico di Torino (Biomedical Lab) and Scuola Superiore Sant'Anna (Soft Mechatronics for BioRobotics Laboratory of the BioRobotics Lab). The aim of this work is the development of a totally polymeric and conductive material for vocal fold models that satisfies three main requirements: i) stretchability in the physiological range of vocal folds, ii) biocompatibility for potential *in vivo* applications and iii) electrical conductivity for electroglottography studies as a method of validation of the model.

The proposed strategy involves the blending of a silicone elastomer with poly(3,4-ethylenedioxythiophene:poly(styrene sulfonate) (PEDOT:PSS), with the addition of Triton X-100 as surfactant and Ethylene Glycol as dopant. First, PEDOT:PSS was blended with polydimethylsiloxane (PDMS), but results were non homogenous and strong phase separation was observed, supposedly due to the long curing time of PDMS. Another commercial silicone elastomer, Silbione RTV4524 (RTV4524), with shorter curing time was used. Different blends were prepared by mixing RTV4524 with PEDOT:PSS, varying the silicone/conductive polymer ratio. Triton X-100 and Ethylene Glycol were kept constant at 1% v/v and 7% v/v, respectively, with respect to PEDOT:PSS. More homogeneous results were achieved for every formulation tested. Two different formulations of the blend (2/1 and 1.5/1 ratios) were chosen and underwent further characterizations. Surface characterization such as ATR-FTIR analysis revealed the presence of PEDOT:PSS absorption bands in the surface, whereas the blends maintained an hydrophobic behaviour, with water contact angle values comparable to those of the pristine silicone:  $109.8^\circ \pm 5.2^\circ$  and  $109.7^\circ \pm 6.2^\circ$  for 1.5/1 and 2/1 ratios, respectively). Preliminary results from uniaxial tensile tests at break revealed that the presence of PEDOT:PSS in the blends led to a decrease in mechanical properties compared to

pristine RTV4524, however still being able to elongate more than 7 times their original length before break. Uniaxial cyclic mechanical tests (100 cycles, strain range 0-40%) showed that both 2/1 and 1.5/1 formulations were capable of cyclic elastic deformation without any decrease in performances. For each case, the Young's moduli were comparable to that of natural vocal folds, with values of  $85.6 \pm 11.8$  and  $59.9 \pm 2.9$  KPa for 2/1 and 1.5/1 ratios, respectively. Indirect cytotoxicity test through resazurin assay revealed that both blends showed no cytotoxic effects after 24, 48, and 72h, with more than 85% viability at the last time point, compared to those of the controls.

Electrical conductivity of the blends is currently under investigation: electromechanical tests are being conducted in order to evaluate if the blends show an appropriate conductivity that would make them suitable for the specific application.

# 1 Introduction

## 1.1 Anatomy of the larynx

The human larynx is a hollow, triangle-shaped organ located in the anterior neck at the level of the C3–C6 vertebrae and it is made up of a set of articulated cartilage structures held together by ligaments and muscles. It connects the hypopharynx (i.e. the inferior part of the pharynx) with the trachea. The larynx extends vertically from the tip of the epiglottis to the inferior border of the cricoid cartilage [1]. It is an organ belonging to the respiratory system that allows the passage of air, speech through the vibration of the vocal cords and it is responsible for protecting the trachea during swallowing thanks to the epiglottis. The larynx, while undergoing individual variations and in relation to age and sex, is on average 4 cm long, 4 cm wide and has an anteroposterior diameter of 3.6 cm [2].

### 1.1.1 *Cartilages*

The laryngeal skeleton consists of nine different types of cartilage (Figure 1.1) joined together and to adjacent structures through membranes that fill the intercartilaginous spaces, and ligaments that provide functional connections.

Three of the nine cartilages are unpaired:

- Thyroid cartilage: the biggest one, shield-shaped, forms the superior, anterior and lateral parts of the larynx;
- Cricoid cartilage: a ring located between the thyroid cartilage and the trachea;
- Epiglottis: a spoon-shaped piece of cartilage that allows the closing or opening of the larynx during breathing or swallowing, respectively.

The other six cartilages consist of 3 pairs:

- Arytenoid cartilages: small pyramidal cartilages located at the posterosuperior border of the cricoid cartilage, they influence the position and tension of the vocal folds;
- Corniculate cartilages: they form the apex of arytenoid cartilages;
- Cuneiform cartilages: club-shaped, located anterior to the corniculate cartilages.

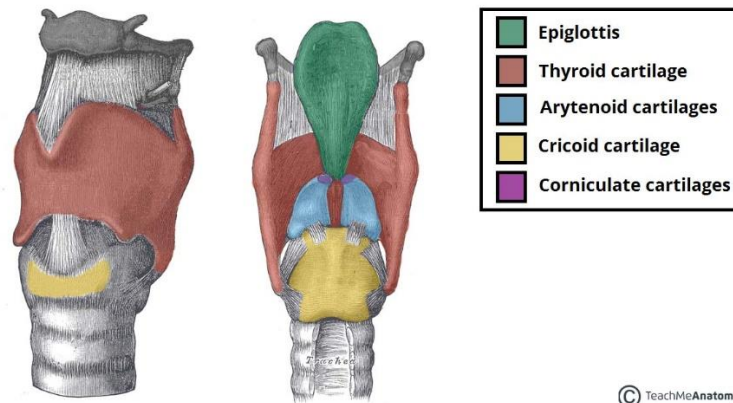


Figure 1.1: Cartilages of larynx.

## 1.1.2 Muscles

The muscles of the larynx can be divided into extrinsic and intrinsic; the former (sternothyroid, omohyoid, sternohyoid, inferior constrictor, thyrohyoid, digastric, stylohyoid, mylohyoid, geniohyoid, hyoglossus, genioglossus) have origin or insertion outside the larynx, on bony parts or on nearby organs, and support and position the larynx within the mid-cervical region; intrinsic muscles originate and are inserted on the structures of the laryngeal skeleton (Figure 1.2). The intrinsic musculature intervenes in the performance of the phonatory functions, modifying the position and/or the length of the vocal folds, which is why a more detailed description is given:

- Cricothyroid: Their action is to bring the upper edge of the cricoid cartilage closer with the lower one of the thyroid cartilage, causing elongation of the vocal folds. Due to their action, the cricothyroid muscles are the tensors of the vocal folds.

- Posterior cricoarytenoid: Their action is to rotate the arytenoid cartilage backwards and outwards by spreading the vocal folds. This results in abduction, lengthening and thinning of the vocal folds.
- Lateral cricoarytenoid: The contraction of these two muscles carries the muscular processes of the arytenoids laterally and the vocal processes medially. This determines a constriction of the *rima glottidis*, lowering, lengthening and thinning the vocal folds.
- Thyroarytenoid: It is possible to distinguish a lateral bundle, constrictor of the glottis and adductor of the vocal folds, and a medial one called vocal muscle. A contraction of the lateral bundle adducts the vocal folds, while the vocal muscle is a tensor of the vocal folds.
- Interarytenoid: It is the only unpaired and median muscle and consists of oblique and transverse bundles. The oblique arytenoid muscles narrow the laryngeal inlet by constricting the distance between the arytenoid cartilages; the transverse arytenoid muscle brings the two arytenoid cartilages closer without making them rotate, resulting in adduction of the vocal folds.

### Intrinsic Muscles of Larynx Lateral Dissection

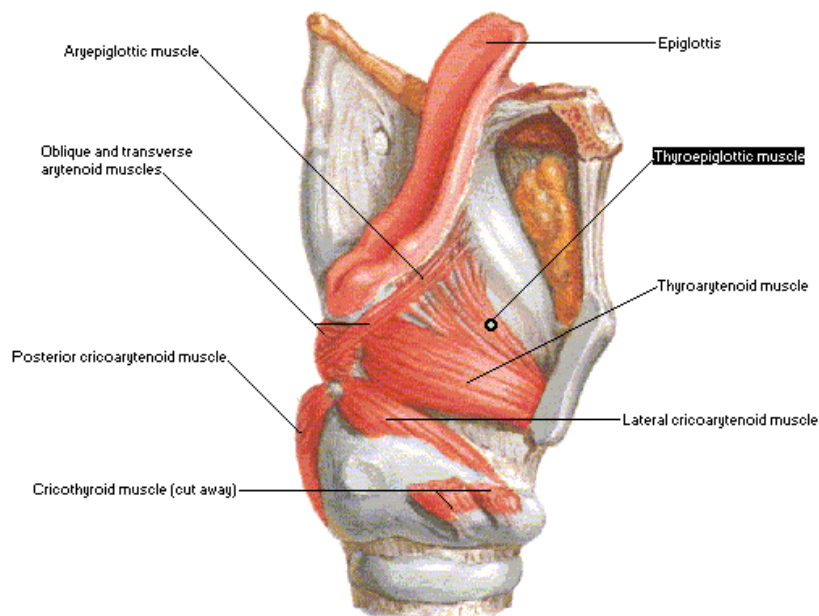


*Figure 1.2: Intrinsic muscles of larynx*

### 1.1.3 Vocal Folds

The voice is the sound produced by the larynx thanks to the vibration of the vocal folds (also called vocal cords) due to the air exhaled from the lungs during the glottal occlusion phase. The vocal folds (Figure 1.3) are an anatomical structure composed of two bands of collagen and elastic tissue covered by a mucous membrane, arranged horizontally inside the larynx and subtended by the vocal or thyroarytenoid muscle. The vocal folds vibrate under the effect of pressure air coming from the lungs, thus generating the fundamental frequency: it is the mucous membrane of the vocal fold that vibrates thanks to its unique vibratory properties, not found in any other body district. The chordal vibration is closely linked to the histological structure of the vocal fold as a whole and, in particular, to the mucous membrane that covers it [1].

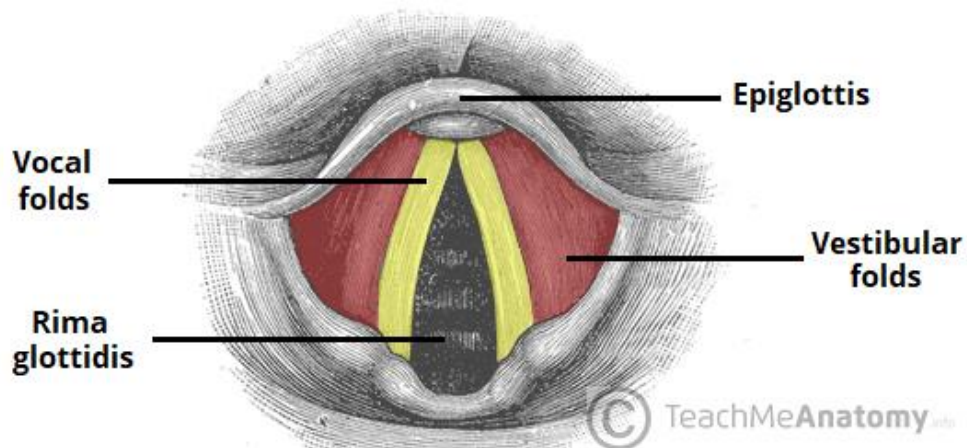


Figure 1.3: The vocal folds.

Hirano proposed the “cover-body” theory, considering the vocal fold as a structure formed by three different superimposed layers: cover (external), transition (intermediate) and body layer (deep) (Figure 1.4) [3].

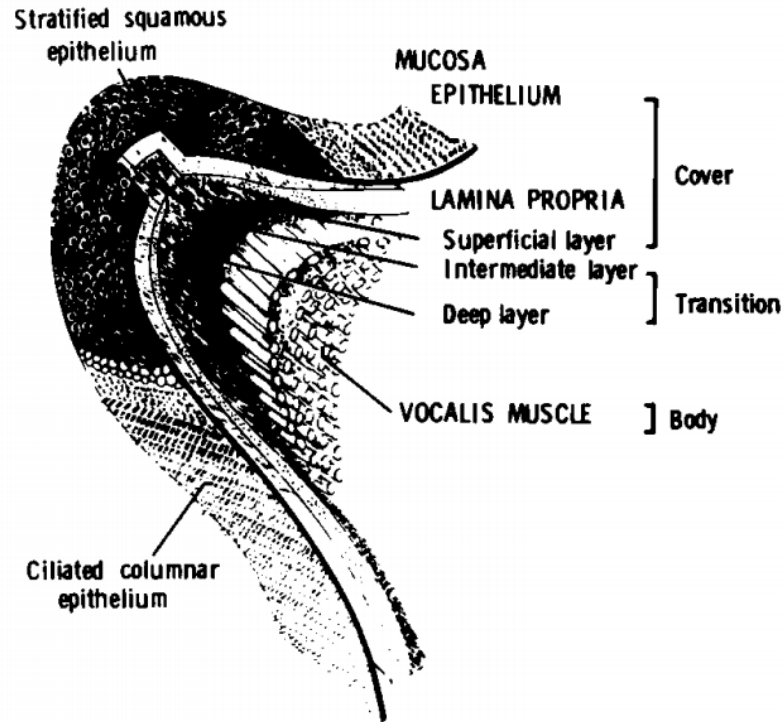


Figure 1.4: The “cover-body” model proposed by Hirano [3]

The cover is formed by the epithelium and the superficial layer of the lamina propria; the transition layer comprises the vocal ligament, the intermediate and deep layer of the lamina propria; the body is uniquely formed by the vocal muscle (thyroarytenoid).

From a biomechanical point of view, the epithelium behaves like a fine capsule delineating the shape of the vocal cord, the superficial layer of the lamina propria is compared to a mass of gelatine, while elastic fibres of the ligament are compared to rubber bands and collagen fibres to a cotton thread. When under contraction, the muscle has a consistency similar to a hard rubber band.

Therefore, the thickness of the vocal cord is characterized by a gradient of stiffness and elasticity: stiffness progressively increases from the superficial layer to the muscle while the elasticity increases from the muscle to the superficial layer. The transition layer is capable of yielding under longitudinal forces without being damaged and with characteristics of rigidity and elasticity that allows the cover to vibrate [3].

## 1.2 Vocal folds models

Located between the lungs and oral and nasal passageways, the vocal folds play a fundamental role in speech production, respiration, and airway protection. Considering the importance of the vocal folds, their damage or loss of control due to trauma, neuromuscular disorders, or laryngeal cancer can have considerable negative impacts on an individual's quality of life.

Wishing to improve treatment options for those individuals, many researchers have been conducting studies to better understand vocal fold tissue properties and anatomy [4,5], investigate vocal fold tissue dynamics during sound production [6,7], as well as efforts related to the development of synthetic vocal fold models [8,9], in order to bring out the different behaviours of healthy and pathological cases.

Considering the difficulty of analysing vocal folds dynamics *in vivo*, researchers conducted studies using excised larynx samples. Many early studies used canine larynges as a common model of phonation and investigated flow characteristics through the glottal channel as well as canine vocal fold impact stresses [10,11]. More recently, researchers have opted to use excised porcine larynges [6,7] which are supposed to have more similar vocal fold structure to human vocal folds than other species [4,5].

While canine, porcine, or other species larynx samples are easily obtainable and cheaper than cadaveric samples, they are also limited by a relatively short time frame during which the samples can be used for experimental testing. Furthermore, it could be difficult to keep track of changes in mechanical properties or in geometry between samples when analysing experimental results. For these reasons, among others, some researchers decided to focus on the development and use of synthetic vocal folds as models of phonation.

In the first synthetic vocal fold studies, such as [12], researchers obtained polyester resin models of a simplified glottal channel to better understand and compare results to a mathematical model describing the fluid flow through the larynx.

Other studies used rubber models to represent an isotropic cover layer of the vocal folds and investigate the change that vocal fold dynamics undergo when varying air flow characteristics and vocal fold geometry [8,13,14].

More recently, Murray et al. described the procedure used to obtain a multi-layer synthetic vocal fold model, made of different silicones, which could approximate the variation in mechanical properties of human vocal folds [9]. In this study it is shown that the multi-layer vocal fold model exhibited a lower phonation onset pressure than single-layer synthetic models and, consequently, more closely approximated human vocal fold dynamics.

Another research group has observed the differences in synthetic vocal fold dynamics due to both linear and nonlinear elastic materials used in the cover layer, concluding that nonlinear models seem to more accurately represent the human vocal folds than linear models do [15].

Electroglottography is a non-invasive, simple and repeatable technique used to study the movement of the vocal folds; it is based on the principle that an alternating electric current, crossing the larynx through two electrodes placed on the sides of the thyroid cartilage, encounters a variable impedance, that depends on the relative position of the two vocal folds. This impedance will be smaller the more the vocal cords are in contact and greater the more distant they are [16]. Moreover, the use of electrically conductive vocal folds prostheses for *in vivo* applications could allow electroglottography to be used as a method of validation to establish if their functioning is comparable to a physiological or pathological case. Syndergaard and Thomson obtained electrically conductive silicone vocal fold replicas by coating them with conductive graphite and showed that electroglottography can be used to monitor their vibration [17].

Despite the undeniable progress made in ameliorating synthetic vocal folds models, these are solely used for performing *ex vivo* tests to underline their mechanical and vibrational properties. To date, the replacement of damaged vocal folds with prostheses has never been achieved. The two main requirements vocal fold prostheses should meet for implantation are biocompatibility and an adequate electrical conductivity.

*In vivo* vocal fold prostheses would most likely manifest the same problematics as laryngeal voice prostheses, considering that the biological environment they would be surrounded by is similar. Silicone voice prostheses are indeed subject to bacterial infections and subsequent biofilm formation, as they are continuously exposed to air flows and an aggressive environment. The biofilm is a biological structure that adheres to the biomedical device, consisting of a multicellular community encapsulated in a matrix of polysaccharides and proteins. Once a mature biofilm has

developed, the bacteria that grow inside it become highly resistant to antimicrobial agents and to immune system. Hence, preventing biofilm formation is of critical importance for the success and maintenance of the functionality of implantable prostheses [18].

### 1.3 Conductive Polymers

Conductive polymers are a class of organic electrical conductors that benefits of several characteristics such as high chemical stability, good conductivity/weight ratio, ease and low cost of production. Furthermore, belonging to the most versatile class of materials, they can be suitably processed and subsequently functionalized to obtain or improve the desired properties, such as wettability, roughness, biodegradability and biocompatibility, for a specific application. For these reasons they represent an interesting class of materials for biomedical applications such as biosensors, drug delivery systems, biomedical implants and tissue engineering. However, their processability and mechanical properties can be quite poor.

Conductive polymers can be divided according to the conduction mechanism into i) ionic conductive polymers and ii) electronic conductive polymers; the latter are further classified as intrinsically or extrinsically conductive (Figure 1.5). Ionic conductive polymers show conductivity due to the mobility of the ions within the polymer network or those formed when polyelectrolytes are added to the solution; electronic conductive polymers are characterized by a high mobility of electrons resulting from constitutive bonds between atoms (intrinsically conductive) or by the presence of conductive particles (extrinsically conductive) [19].

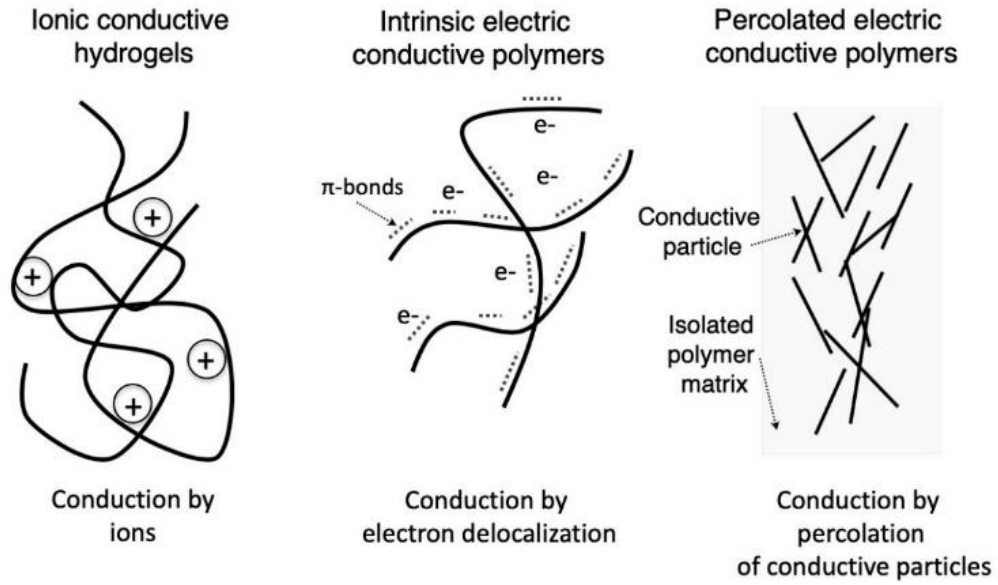


Figure 1.5: Types of conductive polymers

### 1.3.1 Intrinsically Conductive Polymers

The polymer structure of intrinsically conductive polymers (ICP) consists of molecules with conjugated bonds. The conjugation of bonds (Figure 1.6) is the alternation of single and double bonds between carbon atoms along the polymer chain, which represents the fundamental factor for the electrical conduction of these polymers [19].

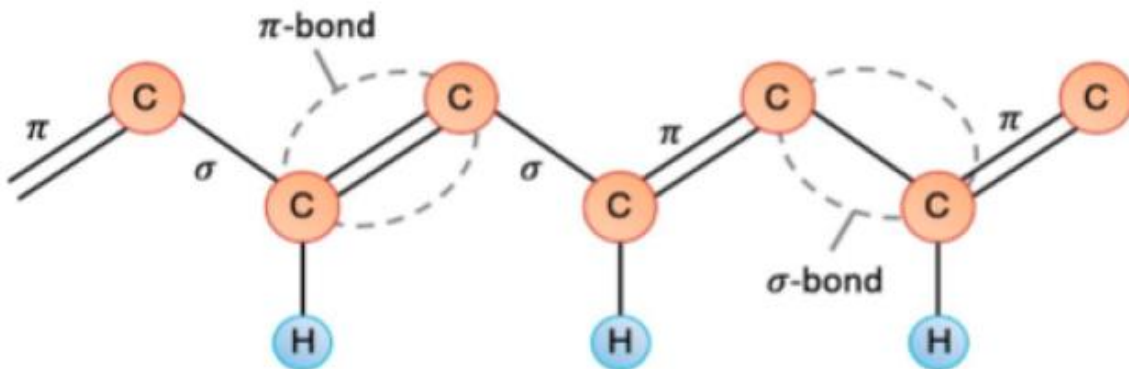


Figure 1.6: Conjugation of bonds formed by alternating single and double bonds [19].

The carbon atom has four valence orbitals and can have different types of hybridization; if a conjugate bond is present, the carbon is hybridized in the form  $sp^2$  (Figure 1.7) [19]. In this form, three of the four orbitals are arranged in one plane, forming a  $120^\circ$  angle and creating strong  $\sigma$ -bonds, while the fourth p orbital forms a weaker  $\pi$ -bond with the other carbon atoms, perpendicular to the plane.

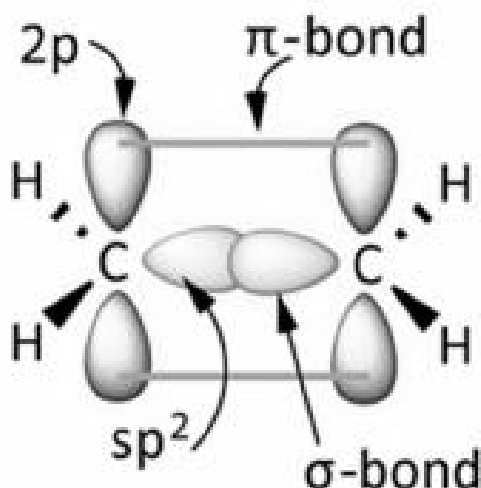


Figure 1.7: Electronic configuration of a double bond

The p orbitals of all adjacent atoms overlap, forming  $\pi$ -bonds with orbitals that extend to the whole chain; as a consequence, electrons are delocalized on the whole macromolecule. This property is essential for the electric conductivity.

The alternation of single and double bonds efficiently decreases the forbidden band between the valence band and the conduction band, up to a level of around 1.5 eV, allowing conjugated polymers to be compared to semiconductors [20].

Although the electrical conductivity is higher with respect to saturated polymers (i.e. polymers where all carbon atoms are bound to four other atoms), it is some orders of magnitude lower than the conductivity of semiconductors. Therefore, it is necessary to use doping, an effective method that allows ICP to achieve electrical properties similar to those of semiconductors [21]. This method allows electrons to flow along the chains thanks to the formation of an intermediate band between conduction and valence bands. Electrons are in fact weakly bound to their atoms, thus able to jump from one polymer chain to another, generating a current when subjected to a potential difference.

During the doping process, an organic polymer, which as an insulator or semiconductor has a typical electrical conductivity in the range of  $10^{-10}$  -  $10^{-5}$  S·cm<sup>-1</sup>, is converted into a conductive polymer with a conductivity range of 1 -  $10^4$  S·cm<sup>-1</sup> [21].

The process of adding the dopant material, typically below 10% in volume, takes place in a non-stoichiometric way, with polymer/doping agent ratio ranging between 5:1 and 15:1. This involves a significant change in the electronic, electrical, magnetic, optical and structural properties of the polymer. Doping is typically a reversible process and it is possible to reproduce the same starting polymer with small variations, without degradation of the polymer chain [21].

Almost all intrinsically conductive polymers are doped through a redox reaction by *p* or *n* type doping. If an electron is removed from the system through an oxidizing doping agent (*p*-doping), a free radical with a positive charge (radical cation) is produced; if an electron is added to the system through a reducing doping agent (*n*-doping), a free radical with a negative charge (radical anion) is produced. Among the two doping techniques, the *p*-doping is the most widespread. Consequently to *p*-doping, a spatial distortion is generated around the area where the reaction occurs, due to the greater amount of energy that remains on the portion of the chain. Distortion of the crystal lattice surrounds and localizes the electrical charge and, together with the combination of the radical cation generated, a structure called polaron is formed. The presence of a polaron allows for electrical conductivity, as it creates a new electronic state located in the forbidden band, with smaller energy than the conduction band, but greater than the valence band (Figure 1.8) [20].

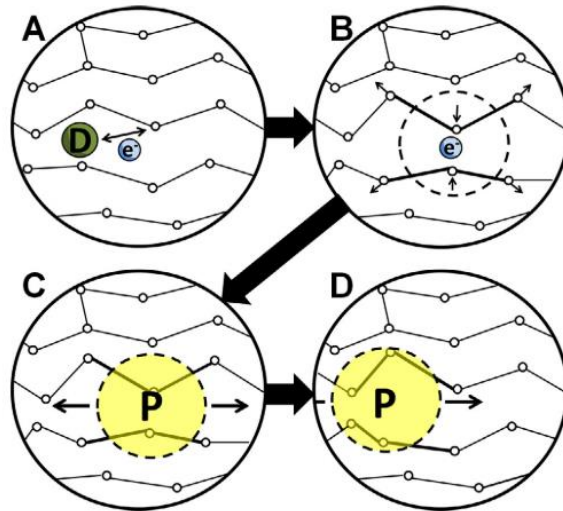
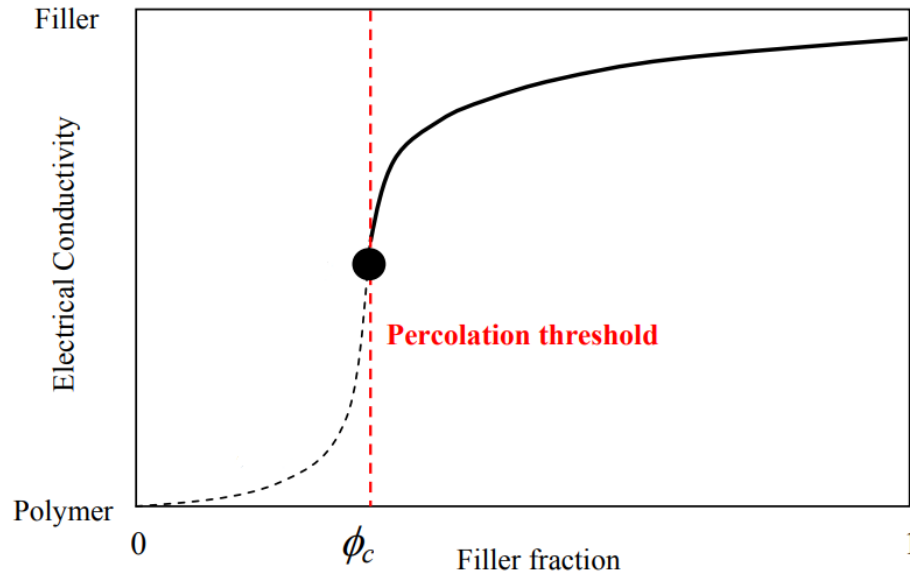


Figure 1.8: Schematic of the doping process within a polymer. *D* represents the dopant, which gives or takes an electron to/from the polymer chains, allowing the creation of a polaron. The polaron, subjected to a potential difference, moves along the chains, allowing for electrical conduction [20].

### 1.3.2 Extrinsicly Conductive Polymers

The majority of polymers behaves like electrical insulators; a method of converting them into conductive materials is to form a composite by adding conductive particles, obtaining extrinsically conductive polymers (ECP). To properly combine conductive fillers and polymers it is necessary to understand the interactions that occur at the micro and nanometric scale with the polymer matrix. The main factors that regulate these interactions depend on the characteristics of the chosen filler, such as its conductivity, shape, size, surface morphology, orientation and dispersion within the matrix, which is strongly related to the production process of the composite [19].

When the quantity of the dispersed conductive particles is such that they are adjacent to each other, a continuous three-dimensional lattice is formed inside the polymer matrix. Indeed, the lattice formation depends on percentage, geometry and dispersion of the filler. The percentage of filler at which the transition from insulating to conductive behaviour of the material occurs is called percolation threshold (Figure 1.9). Below the percolation threshold, the conductivity of the material is low, but suddenly and significantly increases above that value, when the conductive particles come into contact [22].



*Figure 1.9: Electrical conductivity of a composite as a function of the volume quantity of filler inserted into the matrix. The achievement of the percolation concentration allows the electrical conductivity of the composite [23].*

An important parameter that regulates the percolation threshold is the aspect ratio: fillers with a low aspect ratio, i.e. with approximately a spherical form of the particles, have a high percolation threshold value; fillers with a high aspect ratio, on the other hand, have greater specific surface area and consequently a lower percolation threshold value [23]. Furthermore, the dimensions of the filler are also fundamental in lowering the percolation threshold: graphene and nanotubes with nanometric dimensions, for example, are more prone to the formation of an interconnected lattice between particles than a micrometric filler such as carbon black.

Conductive particles do not necessarily need to be in contact with each other: it is possible to have electrical conduction even below the percolation threshold. This occurs when an electron hops from a conductive nanoparticle to another adjacent one, when the distance between them is sufficiently small [24].

An interesting class of ECP is based on dispersion of carbon-derived micro and nanoparticles, such as graphene, carbon nanotubes (CNT) and carbon black [19]. Characterized by a high intrinsic electrical conductivity, these fillers can greatly improve the electrical properties of the polymeric matrix by forming a continuous three-dimensional lattice inside it.

### 1.3.3 *Ionic Conductive Hydrogels*

The term hydrogel refers to a three-dimensional polymeric network capable of absorbing high volumes of water thanks to its hydrophilic properties. Being also characterized by soft consistency and high porosity, hydrogels are often chosen to mimic natural living tissues among all other biomaterials [25]. According to the types of bonds that form the network, it is possible to have reversible or permanent hydrogels: the former relies on molecular entanglements, ionic, H-bonding or hydrophobic forces; the latter shows covalent bonds joining the macromolecular chains or cross-linking polymers [19].

Ionic conductive hydrogels exploit their interconnected porosity and high-water content to enable the transport of polyelectrolytes, thus generating ionic currents. There are different factors influencing ionic conductivity: water content, polymer polarity, hydrogel structure, or presence of salt/ions, among others. Furthermore, mobility and concentration of ions play an important role, too. Ionic concentration acquires more relevance when having low-concentration electrolyte solutions, whereas in high-salt solutions it is the mobility of ions that plays a dominant role. Besides polyelectrolytes, the presence of counterions, higher in ionic rather than non-ionic hydrogels, is another parameter that may lead to an increase in conductivity, since mobile counterions in ionic polymers work as charge carriers [19].

## 1.4 Silicones

Silicones are polymeric materials that contain Si-O bonds (Figure 1.10) along the main chain, thus their repeating unit is  $R_2SiO$ . This term was chosen because they were thought to have very similar properties to those of ketones. However, there is a substantial difference between the structure of silico-ketones and that of ketones: the oxygen of ketones is bonded to a single carbon atom, the same thing does not happen for silicones, in which the oxygen atom forms a bridge between two different silicon atoms. The term silicone is nowadays used as a misnomer which indicates not only polymers that have a large number of Si-O bonds, but all polymers containing silicon [26].

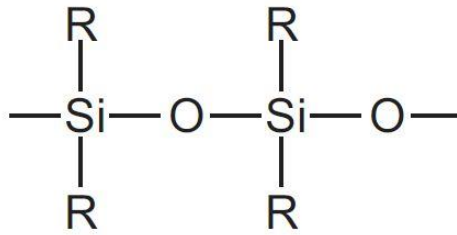
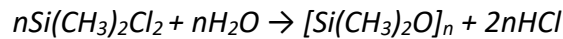


Figure 1.10: Formulation of silicones

One of the most common silicones is polydimethylsiloxane (PDMS, R = CH<sub>3</sub>) which is obtained from the polymerization of siloxanes. By direct reaction between silicon and methyl chloride, dimethyl chlorosilane and other products are obtained and, by subsequent hydrolyzation of dimethyl chlorosilane, linear or cyclic siloxanes are obtained:



Silicones benefit of various properties, such as great thermal stability, resistance to chemical attacks and atmospheric agents, relatively high polymerization kinetic. They are also characterized by good elasticity and optical properties, gas permeability, processability and high thermal and electrical insulation [27].

### 1.4.1 Silicone Elastomers

Silicone elastomers are characterized by molecules that, after curing (i.e. the polymerization process) become interconnected by weak intermolecular bonds, forming very long linear chains; their glass transition temperature  $T_g$  is usually very low (for some of them  $T_g$  is even under -120°C). They also show good tensile properties, given by the flexibility of the chains that deform under the application of a load, stretching rather than breaking: the polymer chains, usually coiled, can change their conformation and stretch when subjected to an external load, aligning to the direction of the force; however, silicone elastomers do not permanently deform: the covalent cross-links between the polymer chains ensure that the elastomer will return to its original configuration when the load is removed. For these reasons silicone elastomers are amorphous, soft and flexible but tough, having

good tear and abrasion resistance, although they may show low mechanical strength at room temperature [28].

The resistance of these elastomers can be improved by adding fillers or reinforcing agents to the system, which increase the mechanical work required to move the chains and therefore the overall mechanical strength [27]. Mechanical properties may vary a lot among different silicone elastomers: depending on the formulation, they can stretch between 150-800% of their initial length and their Young's modulus ranges from 50 KPa to 1-2 MPa [29].

In order to convert it to a solid, a silicone elastomer needs to be cured; the process of curing may vary according to the cure system used: the most used are peroxide, platinum-catalysed and condensation cure systems.

Peroxide curing is widely used for curing silicone elastomers; however, the curing process involves by-products release, which can be an issue in food contact and medical applications.

In a platinum-based silicone cure system, a hydride- and a vinyl-functional siloxane polymer react with the addition of a platinum complex catalyst that creates an ethyl bridge between the two; the reaction has no by-products release. This type of silicone elastomers cures quickly, but the ability of curing can be easily inhibited by the presence of tin, sulphur, and many amine compounds [30].

Condensation cured silicone elastomers can be one-part or two-part systems; they are called room temperature vulcanizing (RTV) silicones and cure in a period ranging from a few minutes to a few hours. In one part systems the curing agent is air humidity, which induces the formation of crosslinks between the main chains and acts on the hydrolysable groups of the oligomer. Two-part silicones consist of cross-linker and condensation catalyst put together in the first part, while the polymer and any fillers or pigments are put together in the second part. Curing occurs by mixing the two parts and the humidity in the air finalizes the polymerization process [27].

### *1.4.2 Biomedical Silicones*

In recent years, silicone rubbers, especially those based on PDMS, have found widespread use for biomedical applications. Their success is mainly due to their properties such as biocompatibility,

chemical and thermal stability, low toxicity and antiadhesive behaviour. Some examples of medical devices that use PDMS are blood pumps, breast implants, oxygenators, finger joints, contact lenses, drug-delivery systems.

From a clinical point of view, in order to be biocompatible, a biomaterial should meet these requirements: (a) the absence of thrombogenic, toxic, allergic or inflammatory reactions; (b) no destruction of formed elements; (c) no change in plasma proteins or enzymes expression; (d) no immunological reactions; (e) no carcinogenic effects; and (f) no deterioration of adjacent tissues [31] [32] [33].

Usually silicone elastomers are not able to meet all the properties listed above, especially when it comes to long-term implants; for this reason, surface or bulk modifications can be made.

Surface modifications are usually made on materials that already possess good bulk properties and can be achieved using physical or chemical techniques [33]. Physical techniques consist in chemical modifications of the surface layer, or in the deposition of additional layers on the surface. Among them the most used for silicones are corona, plasma and laser treatments. As for chemical techniques, the most common methods to chemically modify the surface of silicones are etching, surface oxidation and etching, hydrolysis, functionalization, and surface grafting. Surface grafting is the most used one and, depending on the properties to be provided to the biomaterial, it can be assisted by  $\gamma$ -radiations, corona, plasma or laser treatments.

From a biomedical point of view, surface properties are often of crucial importance, considering that the surface of a biomaterial is the part always being in contact with the biological environment. Silicone-based biomedical devices, despite being known for their high biocompatibility and biodurability, are associated with a likelihood of infections as the silicone's hydrophobic surface is prone to bacterial adhesion and biofilm formation, that may lead to the failure of the implanted device. Several strategies have been investigated for the inhibition of bacterial adhesion and subsequent biofilm formation, but most of them do not seem to be very effective when considering long-term implants. Covalent bonding of biocompatible antimicrobial agents (such as quaternary ammonium silane and antimicrobial peptides) onto the device surface appears promising since they will not be released and the efficacy can be maintained for long-term application [34].

On the other hand, bulk modifications, unlike the superficial ones, aim to obtain a final product that satisfies certain properties, not only the superficial ones, required for a given application. The two most used bulk modification techniques are blending and co-polymerization [33].

Blending consists in the physical combination of two or more structurally different polymers to obtain a new material with additional or improved properties of interest. The parameters that affect blending the most are the mixing thermodynamics and the use of molecules that can improve the interface between the polymers, reducing the surface tension and therefore the phase separation [35].

Copolymerization is the formation of polymer chains composed of two or more different monomer species. Based on how the monomer species are arranged, copolymers can be divided into two categories: statistical, random and alternating copolymers belong to the first, where there are short sequences of the same monomer specie; the second category includes block, graft and segmented copolymers, characterized by long sequences of the same monomer connected to each other [33].

A less common bulk modification technique is the production of an interpenetrating polymer network: it is a combination of two polymers in network form, at least one of which is synthesized and/or cross-linked in the presence of the other. The main advantage of this technique is that it is possible to combine different polymer properties, while at the same time reducing any incompatibility effects [36].

## 1.5 Aim of the Work

This work of thesis was born thanks to the collaboration between Politecnico di Torino (Biomedical Lab) and Scuola Superiore Sant'Anna (Soft Mechatronics for BioRobotics Laboratory of the BioRobotics Lab), with the aim of creating vocal folds models made of a composite silicone-based material with enhanced electrical conductivity. Sant'Anna's BioRobotics Lab is indeed working on the creation of silicone vocal fold models able to emulate the mechanical and anatomical behaviour of physiological and pathological natural vocal folds. Their manufacturing process is based on Hirano's 3-layer cover-body model, characterized by a gradient of stiffness and elasticity from the

outer (cover) to the inner (body) layer: stiffness progressively increases from the superficial layer to the muscle while the elasticity increases from the muscle to the superficial layer.

For this specific application, a silicone-based material that also shows an appropriate electrical conductivity could allow the use of diagnostic tools, such as electroglottography, as a method of comparison between natural and artificial vocal folds: positioning electrodes for the acquisition of an electrical signal from both types of vocal folds and comparing the signals obtained this way would be a simple and effective method to establish if artificial vocal folds behave like physiological or pathological natural vocal folds. For these reasons, this work is focused on the development of a totally polymeric material that should satisfy three main requirements: i) stretchability in the physiological range of vocal folds, ii) biocompatibility to potentially lead the way to an *in vivo* application and iii) electrical conductivity so that one could use diagnostic tools as a method of validation to evaluate its behaviour.

## 2 Materials and Methods

### 2.1 Materials

#### 2.1.1 PEDOT:PSS

Over the last few years, one of the most studied conductive polymers is poly(3,4-ethylenedioxythiophene) (PEDOT) as it is used for a large scale of applications, such as in optoelectronics, in transistors, in electrodes, in super capacitors, in bioengineered tissues and in solar cells, thanks to its high electrical conductivity, optical transparency, mechanical properties of flexibility and torsion, biocompatibility and low cost of production.

PEDOT is intrinsically a semiconductor derived from substitutions in positions 3 and 4 of polythiophene with a dioxyalkylene bridging group (Figure 2.1). This increases the polymer's resistance to degradation by oxygen and water, as well as its electrical and chemical stability, while inevitably decreases its solubility [37].

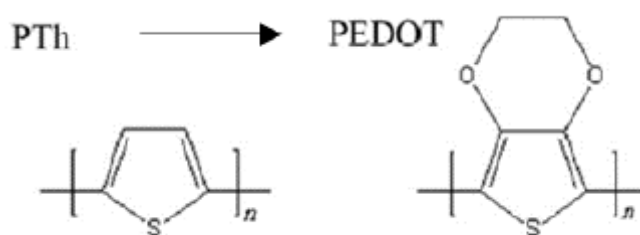


Figure 2.1: Chemical structures of polythiophene (PTh) and PEDOT

Since PEDOT is insoluble in most common solvents, poly(styrene sulfonate) (PSS) is added during the oxidative polymerization of EDOT to increase its solubility. PSS is a water-soluble polymer, capable of promoting the dispersion of PEDOT in aqueous solutions through the formation of a polyelectrolytic PEDOT:PSS complex (Figure 2.2). The PSS within the complex has two main functions: the first is to balance the charge of the PEDOT, acting as a counterion; the second function

is to disperse the polymer chains of PEDOT in water, through the formation of a micro-dispersion of PEDOT particles surrounded by bundles of PSS [38].

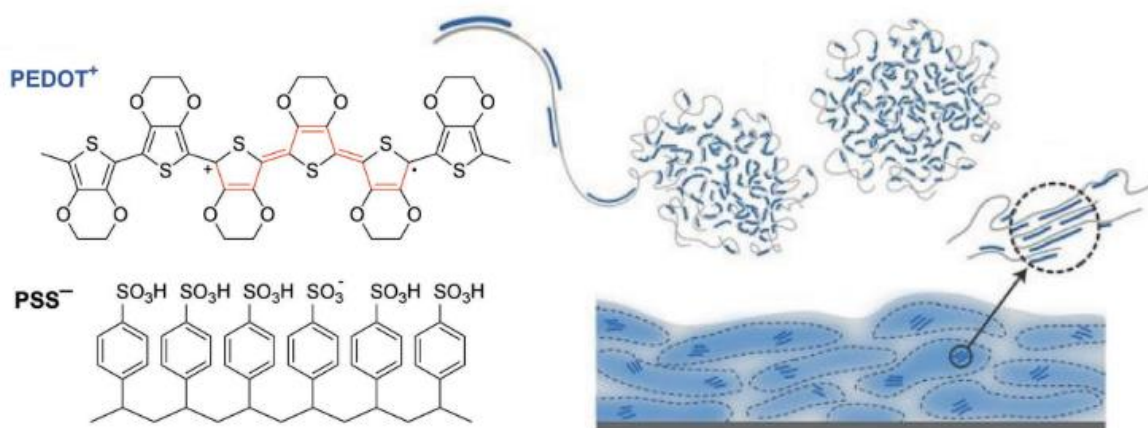


Figure 2.2: Chemical structure of PEDOT:PSS; formation of colloidal gel particles when dispersed in water; microstructure of the resulting films with PSS-rich domains (gray) and PEDOT:PSS-rich domains (blue) [38].

The physical characteristics of PEDOT depend on the morphology, crystallinity and molecular weight. Furthermore, the final properties will also depend on the doping level and the conductivity achieved: light and thermal treatments, as well as the use of secondary dopants, blending with organic solvents (such as ethylene glycol, dimethyl sulfoxide, N,N-dimethyl formamide and tetrahydrofuran), or post-treatments can lead to a great improvement in PEDOT's electrical conductivity, up to hundreds of  $\text{S cm}^{-1}$  [39].

Among other different conductive polymers available in the market, PEDOT:PSS has been chosen because it shows a piezoresistive behaviour: in fact, it is able to vary its electrical resistance when subjected to pressure triggers.

Hereaus Clevios PH1000 was purchased from Ossila: it is an aqueous solution containing 1.0 - 1.3 wt.% of PEDOT:PSS. The PSS to PEDOT ratio is 2.5 and its electrical conductivity ranges from 0.2 to  $1 \text{ S cm}^{-1}$ .

## 2.1.2 Surfactant and Dopant

t-Octylphenoxy polyethoxy ethanol (Triton X-100) (Figure 2.3) was used as a surfactant to lower the interfacial tension between the PH1000 solution and the silicone elastomer, with the aim to obtain a more homogenous blend.

Triton X-100 was purchased from Sigma-Aldrich in the form of a liquid with an average molecular weight of 625 g/mol.

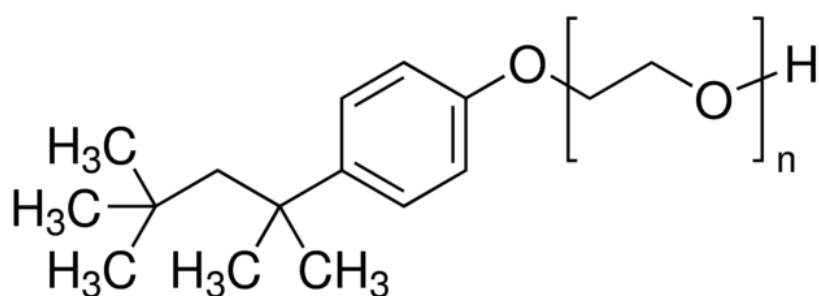


Figure 2.3: Triton™ X-100 chemical structure (courtesy of sigmaaldrich.com)

Ethane-1,2-diol (Ethylene Glycol, EG, Figure 2.4) was purchased from Carlo Erba and used as a dopant to preserve and enhance the electrical conductivity of PEDOT:PSS.

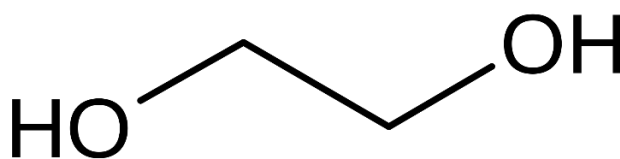


Figure 2.4: Ethylene Glycol chemical structure

### 2.1.3 *Silicone Elastomers*

An industrial medical-grade silicone elastomer, Silbione RTV 4524 (RTV4524) was purchased from Elkem Siliconi Italia srl in the form of two liquid components, a pre-polymer (Part A) and curing agent (Part B). The two components are mixed in a 1:1 weight ratio, either by hand or using a low-speed electric or pneumatic mixer to minimize the introduction of air into the mixture, and the final product cures at ambient temperature (23°C) in around 45 minutes.

SYLGARD 184 Silicone Elastomer Kit was bought from The Dow Chemical Company in the form of two liquid components, a pre-polymer (Part A) and curing agent (Part B). PDMS is obtained by carefully mixing the two liquid components with a weight ratio of 10:1. Curing is carried out at ambient temperature (25°C) for at least 48 hours.

## 2.2 Blends Preparation

Blends of RTV4524 or PDMS and PEDOT:PSS were obtained following the protocol of Luo et al. [40], which was modified to suit the available instrumentation. In order to prepare the polymer blends, PEDOT:PSS, Triton X-100 and EG were mixed with Part A of either RTV4524 or PDMS silicones. On the basis of the PEDOT:PSS volume, the percentage of Triton X-100 and EG were kept constant and equal to 1% v/v and 7% v/v, respectively; the silicone elastomers/PEDOT:PSS ratio was varied, as shown in Table 2.1.

Table 2.1: Volumes of silicone elastomers in relation to PEDOT:PSS' volume and respective blends' shortened names.

SYLGARD (PDMS)	RTV 4524	PEDOT:PSS	Ethylene Glycol	Triton X-100	Shortened Name
0	2	1	7%	1%	R2/P1
0	1.5	1	7%	1%	R1.5/P1
0	1	1	7%	1%	R1/P1
0	1	1.5	7%	1%	R1/P1.5
2	0	1	7%	1%	S2/P1

The solutions were left under magnetic stirring overnight at 300 rpm to obtain homogenous dispersions, then the Part B was added to the solution containing its respective Part A. The blends were then briefly stirred to properly mix the two silicone parts (Figure 2.5).

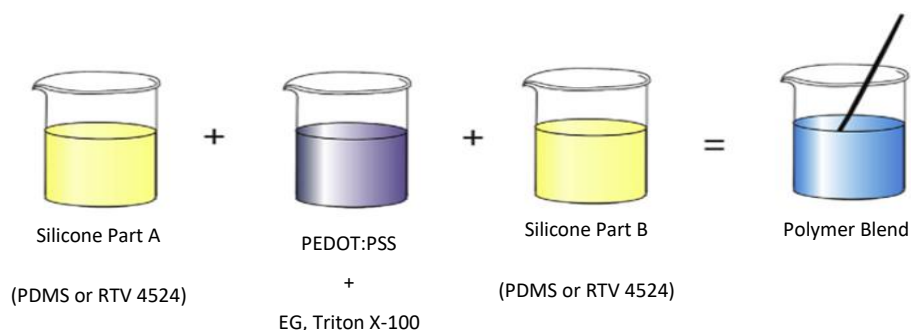


Figure 2.5: Polymer blends preparation

Dog bone-shaped samples were obtained by pouring 2.1 mL of solution into a 3D-printed mold and left curing for 24 hours; the samples collected from the mold (Figure 2.5) had a thickness of 1.9 - 2.8 mm. Rectangle strips of 40 x 10 mm<sup>2</sup> were cut from the samples obtained by pouring 3 or 10 ml of solution into a 55- or 110-mm diameter borosilicate Petri dish, respectively, and left curing for 24 hours; the samples obtained this way had a thickness of 0.7 – 1.1 mm.



Figure 2.6: A) 3D-printed mold for dog bone-sized samples and B) samples dimensions

## 2.3 Mechanical Tests

In order to evaluate the mechanical properties of the different materials, uniaxial tensile tests at break and uniaxial cyclic tests were performed.

### 2.3.1 Uniaxial Tensile Test at Break

Dog-bone shaped samples were tested using an MTS Q-Test 10 machine (Figure 2.7) equipped with a 10 N load cell, using a test speed of 50 mm/min, preload of 0.02 N, and acquisition rate of 100 Hz. Only RTV4524 (n=8) and R2/P1 (n=5) samples were tested.

Samples thickness was recorded before testing, by measuring it three times using a micrometre and mediating among those measurements. The cross-sectional area of each sample, assumed constant during deformation, was calculated by multiplying the thickness by samples central width. The software integrated with the instrumentation provided the values of extension and load measured during testing as output data; the corresponding strain ( $\epsilon$ ) and stress ( $\sigma$ ) values were obtained as follow:

$$\sigma = F/A_0 \text{ [Pa]} \quad \text{[Equation 2.1]}$$

$$\varepsilon = (L-L_0)/L_0 \text{ [mm/mm]} \quad \text{[Equation 2.2]}$$

Where  $F$  is the force expressed in Newton,  $A_0$  is the cross-sectional area expressed in  $\text{mm}^2$ ,  $L$  and  $L_0$  are the final length and the initial gauge length (assumed equal to 10mm for every sample obtained from the mold) expressed in mm of each sample. It was then possible to obtain a stress-strain curve for each sample. From stress-strain curves, the strain and stress at break were calculated from the last values of extension and load provided by the instrumentation, which automatically stopped when breakage was detected. For linear tracts Hooke's Law was assumed to be valid:

$$\sigma = E \cdot \varepsilon \text{ [KPa]} \quad \text{[Equation 2.3]}$$

Young's Modulus ( $E$ ) was then calculated for each sample using a linear regression function (strain range from 0 up to 150% deformation). Data were processed using Microsoft Excel software.

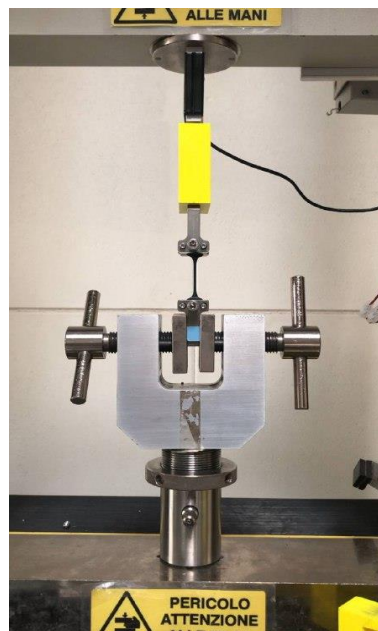


Figure 2.7: MTS Q-Test 10 machine used to perform uniaxial tensile tests at break.

### 2.3.2 *Uniaxial Cyclic Tensile Test*

Rectangle strips (40 x 10 mm<sup>2</sup>) were tested by using TA ElectroForce Planar Biaxial TestBench machine paired with WinTest software (TA instruments, United States). Samples were mounted into 12x12 mm<sup>2</sup> grips along their main direction and stretched at 1 Hz up to 40% of their gauge length for 100 cycles; a 50 KN load cell was used and data were acquired at 500 Hz.

Each sample thickness was recorded before testing, by measuring it three times using a micrometre and mediating among those measurements. The cross-sectional area of each sample, assumed constant during deformation, was calculated by multiplying the thickness by samples central width. The software integrated with the instrumentation provided the values of extension and load measured during testing as output data; the corresponding strain and stress values were obtained using Equation 2.1 and Equation 2.2. Data were processed with MATLAB, filtered to reduce noise. From the stress-strain curves, and considering the full strain range from 0 up to 40% deformation, Young's Modulus  $E$  was then calculated for each cycle of the load curves. The average  $E$  was obtained by mediating the values from all 100 cycles. Stress at maximum deformation ( $\epsilon = 40\%$ ) was evaluated for every cycle and mediated over the 100 cycles for each sample.

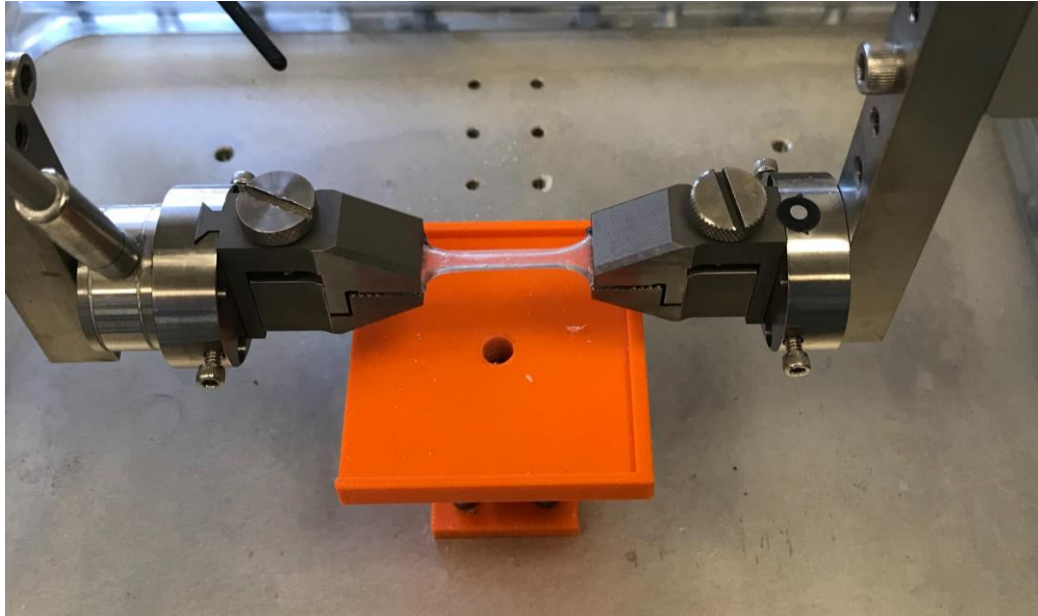


Figure 2.8: TA ElectroForce Planar Biaxial TestBench used to perform uniaxial cyclic tensile tests.

## 2.4 Water Contact Angles Measurements

The contact angle  $\theta_c$  (Figure 2.9) indicates how much a solid material is wettable by a certain liquid, usually water. It is defined by an equilibrium of the interfacial energies between three phases: liquid, solid and gas phase. Being  $\gamma_{SG}$ ,  $\gamma_{SL}$ ,  $\gamma^{LG}$  the interfacial energies between solid-gas, solid-liquid, liquid-gas phases respectively, the Young's equation determines the contact angle  $\theta_c$ :

$$\gamma_{SG} - \gamma_{SL} - \gamma_{LG} \cos(\theta_c) = 0 \quad [Equation 2.4]$$

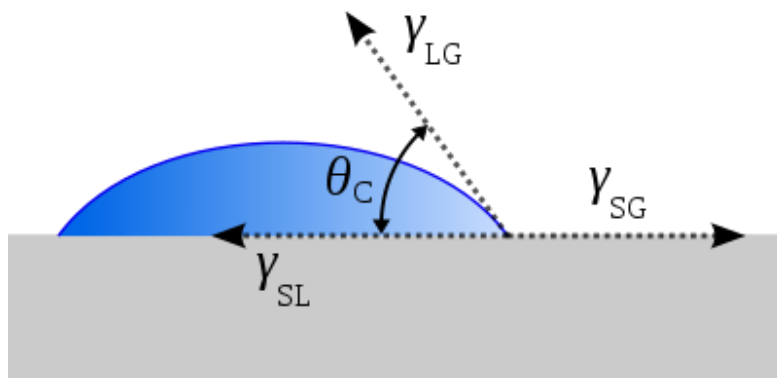


Figure 2.9: Contact angle  $\theta_c$  in relation to the interfacial energies between solid, liquid and gas phases.

Water Contact Angle (WCA) measurements were performed to estimate samples wettability using a Krüss Drop Shape Analyzer. The droplet (2-4  $\mu\text{l}$ ) was deposited on the surface through a needle; left and right contact angles were calculated and mediated directly by the software Drop Shape Analysis to obtain the final value. RTV4524 and RTV/PEDOT:PSS materials were tested in order to evaluate any possible differences in terms of surface wettability.

For each sample, (n=3) distinct measurements were made; data are reported as mean  $\pm$  standard deviation.

## 2.5 ATR Fourier-transform Infrared Spectroscopy

Fourier transform infrared spectroscopy (FTIR) is a non-destructive analysis method for the evaluation of materials chemistry, from the vibrations of chemical bonds. It is based on the absorption of the infrared radiation by materials. A component (spectrometer) focuses the infrared radiation on the sample to measure both the wavelengths absorbed by the material and the intensity of the absorption; a spectrum is then produced through a mathematical operation called the Fourier transform. Spectra can provide both qualitative and quantitative indications: the wavelengths absorbed by the sample are characteristic of the chemical groups present in the sample, while the absorption intensity at a defined wavelength indicates the concentration of the chemical group responsible for the absorption. Attenuated total reflectance (ATR) is an accessory of FTIR spectrometer for the analysis of surface properties of solid or thin film samples rather than their bulk properties, thus having a penetration depth of around 1-2  $\mu\text{m}$ , depending on sample conditions.

Samples were analysed using Nicolet iS50 FT-IR spectrometer (Thermo Scientific, Milano) equipped with an ATR accessory (Smart iTX) after collecting the background signal to be subtracted to each sample's spectrum, in order to minimize the interferences due to the surrounding environment. The scanned wavelengths ranged from 4000 to 500  $\text{cm}^{-1}$ , the number of scans was set at 32, with a scan resolution of 4 $\text{cm}^{-1}$ .

## 2.6 Indirect Cytotoxicity Test

In order to evaluate the potential cytotoxicity of samples, indirect cytotoxicity tests at 24-48-72h time points were performed through the resazurin assay using human HFF1 fibroblasts. When resazurin enters the mitochondria of viable cells it is reduced to resorufin. Being resorufin highly fluorescent, its concentration can be measured through fluorimetry, with an excitation point at 540 nm and an emission point at 590 nm. The higher the fluorescence, the higher the concentration of resorufin and, therefore, the metabolic activity of the cells. The intensity of the signal is hence directly proportional to the number of viable cells. Greater viability implies poor cytotoxicity of the material.

Cells were routinely cultured in DMEM (Dulbecco's Modified Eagle Medium), supplemented with 15% of FBS (foetal bovine serum), 2% of glutamine and 1% of penicillin and streptavidin antibiotics. Cells were then seeded in a 96-plate multiwell with two different cell densities:  $1 \times 10^4$  cells/well and  $2 \times 10^4$  cells/well and let adequately attach for 24 hours before the beginning of the test. Three different conditioned media were prepared by submerging 1 mg/mL of material (UV-sterilized) in the culture media for 24 h. RTV4524, R2/P1 and R1.5/P1 were used to prepare conditioned media. After 24h, not-conditioned culture medium was removed from each well and substituted with conditioned medium. Control samples (CTRL) were prepared by substituting the medium with fresh medium. After 24 h, medium was discarded and replaced by 120  $\mu$ l of fresh medium containing 20  $\mu$ l of resazurin solution to perform the resazurin assay. Cells were then incubated at 37°C for 4 hours before the reading. Then, the emission was detected using a Biotek plate reader. Samples were tested in triplicates; results are reported as mean  $\pm$  standard deviation.

After the reading, the medium containing resazurin was removed from each well and substituted with fresh conditioned medium that was left in contact with cells for other 24h, in order to perform the same test for the next time point at 48h; the same procedure was repeated for the last time point at 72h.

## 2.7 Statistical Analysis

Statistical analysis was performed to compare the different materials used in the tests that will follow, in order to state whether they showed similarity or not. GraphPad Prism software was used, where t-test, one-way and two-way ANOVA tests were carried out. For every type of test, the alpha threshold was set at  $\alpha=0.05$ , corresponding to a 95% confidence interval. Multiple comparisons tests were performed by using Tukey's statistical hypothesis testing. Depending on the P value calculated, it will be represented in the results as "ns" (not significant, i.e., the two entities being compared are similar), if  $P > 0.05$ , or as a variable amount of asterisks: \* if  $P < 0.05$ , \*\* if  $P < 0.01$ , \*\*\* if  $P < 0.001$  and \*\*\*\* if  $P < 0.0001$ .

### 3 Results and Discussion

The first part of this work focused on the optimization of the protocol to obtain an homogenous blend, using two different silicone elastomers (PDMS and RTV4524) and varying their concentration in relation to the amount of PEDOT:PSS, as already shown in Table 2.1. At first, blends were prepared by using PDMS (S2/P1). Unfortunately, it was not possible to achieve the same results previously obtained by Luo et al. [40]. As shown in Figure 3.1, PEDOT:PSS and PDMS showed a noticeable phase separation, i.e. non-homogeneity of the blend.



*Figure 3.1: S2/P1 blend after curing.*

The cause of non-homogeneity could have consisted in the elevated curing time of PDMS.

Therefore, PDMS was replaced with RTV4524, another medical-grade silicone elastomer capable of curing in way less time, i.e. 45 min.

Homogeneity results for each blend tested using RTV4524 are reported in Table 3.1. It was not possible to achieve homogeneity all blends prepared: as the PEDOT:PSS to RTV4524 ratio increased, the blends tended to show remarkable phase separation that made them unsuitable for testing (see Figure 3.2).



Figure 3.2: A) Non-homogenous and B) homogenous RTV4524/PEDOT:PSS blends after curing.

For this reason, homogenous blends only were selected for further testing: R2/P1 and R1.5/P1, as shown in Table 3.1. Pure RTV4524 was used as a reference for both blends.

Table 3.1: Homogeneity of the different blend formulations produced.

SYLGARD (PDMS)	RTV4524	PEDOT:PSS	Ethylene Glycol	Triton X-100	Homogeneity
0	2	1	7%	1%	Yes
0	1.5	1	7%	1%	Yes
0	1	1	7%	1%	No
0	1	1.5	7%	1%	No
2	0	1	7%	1%	No

### 3.1 Uniaxial tensile test at break

Uniaxial tensile test at break was performed as a preliminary test, where (n=8) samples from RTV4524 and (n=5) samples from R2/P1 were tested, as shown in Figure 3.3.

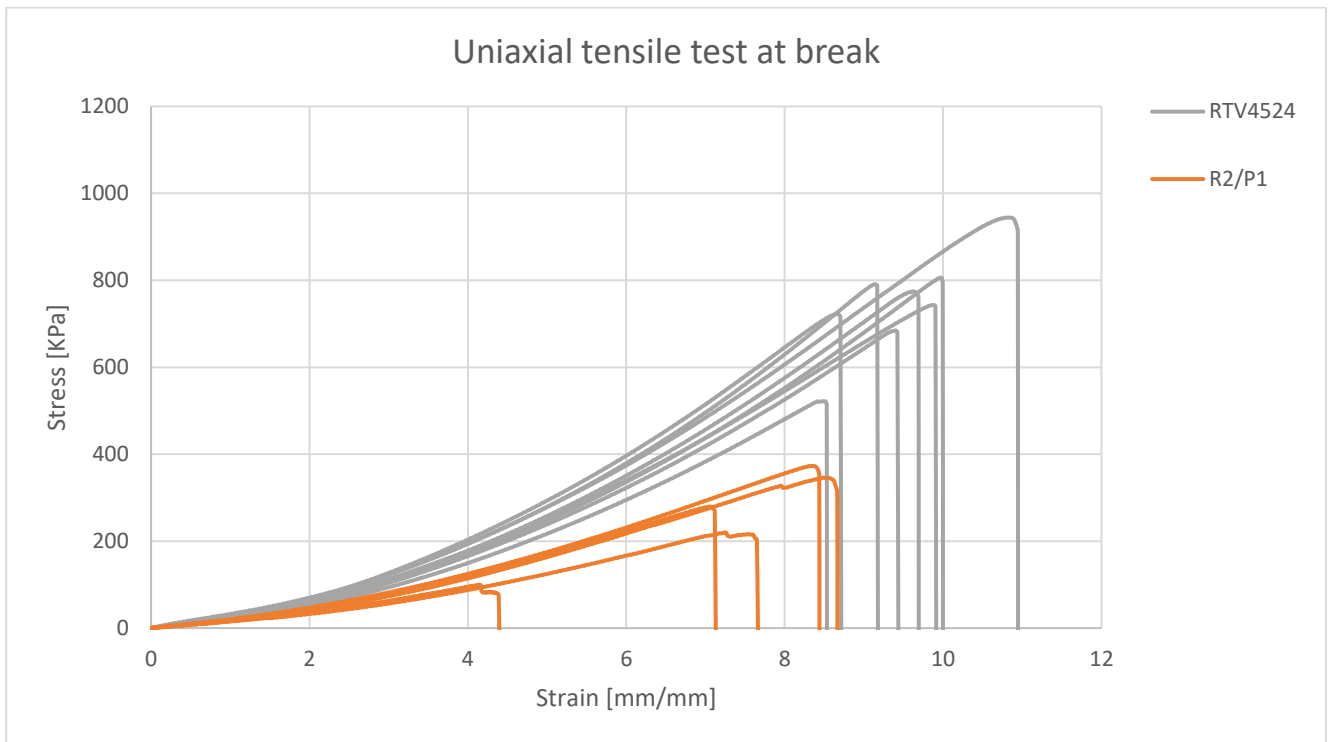


Figure 3.3: Uniaxial tensile test at break for RTV4524 (n=8 samples, in grey) and R2/P1 (n=5 samples, in orange).

Stress and strain at break, as well as Young’s modulus (considering the deformation range from 0% to 150% strain) were evaluated as previously discussed in 2.3.1. The results are shown in Figure 3.4, Figure 3.5 and Figure 3.6, respectively, reported as mean  $\pm$  standard deviation.

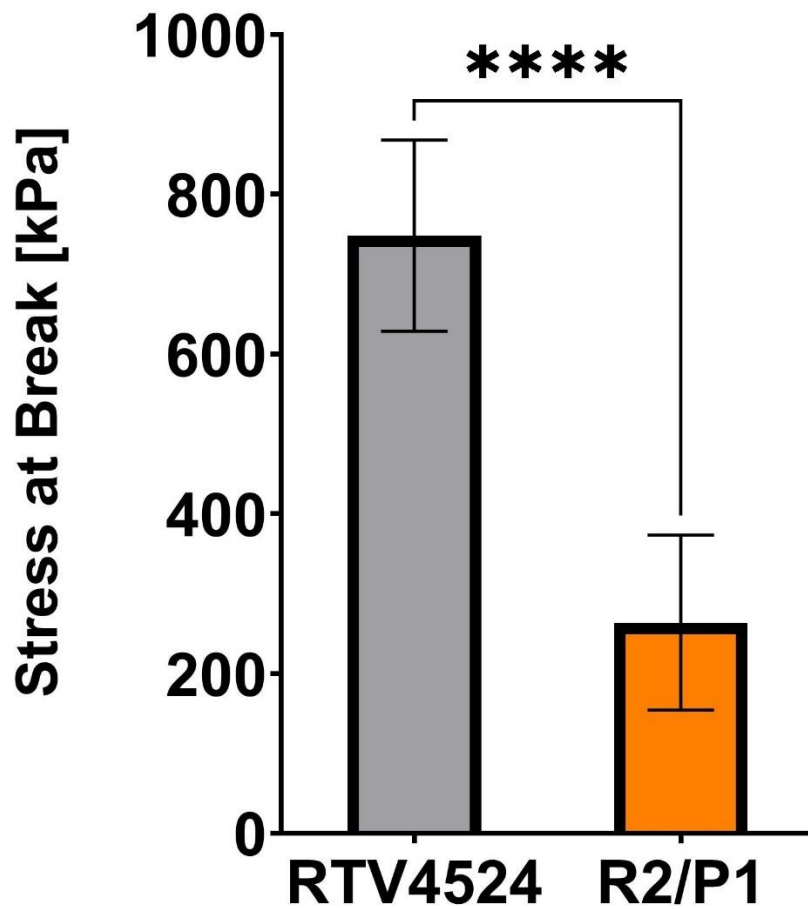


Figure 3.4: Average stress at break for RTV4524 (grey) and R2/P1 (orange) samples.

As it is possible to observe, the average stress at break for RTV4524 samples was  $749 \pm 120$  KPa, considerably higher with respect to  $264 \pm 110$  KPa of R2/P1: the pristine silicone elastomer showed a better capability of resistance to loads before breaking than the blend. Unpaired t-test between the two materials revealed that they were significantly different ( $P < 0.0001$ ).

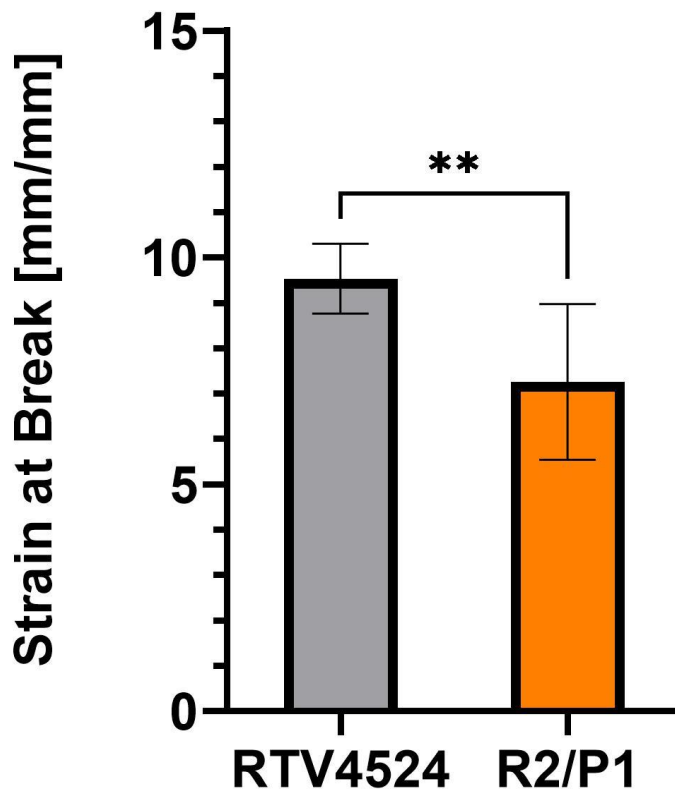


Figure 3.5: Average strain at break for RTV4524 (grey) and R2/P1 (orange) samples.

The results show that the average strain at break measured was  $9.6 \pm 0.8$  mm/mm and  $7.3 \pm 1.7$  mm/mm for RTV4524 and R2/P1, respectively: this shows that blending with PEDOT:PSS reduced the elasticity of the material, which is less able to elongate until breakage. Unpaired t-test between the two materials revealed that they were significantly different ( $P = 0.0068$ ).

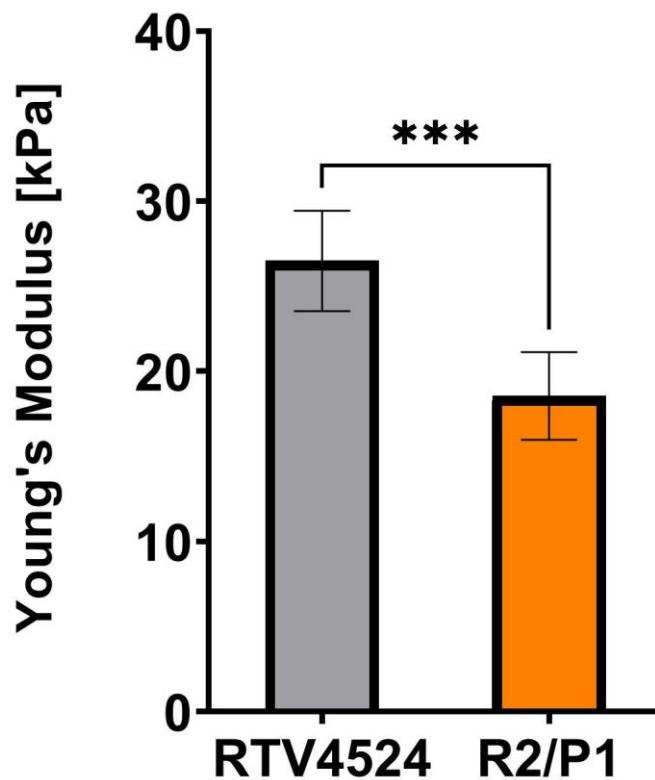


Figure 3.6: Average Young's modulus for RTV4524 (grey) and R2/P1 (orange) samples, obtained considering the deformation range from 0% to 150% strain.

The average Young's modulus is  $26.5 \pm 2.9$  KPa and  $18.6 \pm 2.6$  KPa for RTV4524 and R2/P1, respectively: pure silicone elastomer appears stiffer than the blend. Unpaired t-test between the two materials revealed that they were significantly different ( $P = 0.0004$ ).

The results reveal that blending RTV4524 with PEDOT:PSS has a clear impact on the mechanical properties with respect to pristine silicone elastomer: the blend is softer, less elastic and not able to sustain the same load before breaking. However, natural vocal folds physiological strain usually does not exceed 0.4-0.5 mm/mm [41], that is significantly smaller than the strain at break for R2/P1. For this reason, this blend was considered suitable for the specific application and different RTV4524/PEDOT:PSS ratios were tried.

## 3.2 Uniaxial cyclic tensile test

Curves from uniaxial cyclic tensile tests were obtained by testing RTV4524 (n=5), R1.5/P1 (n=3), and R2/P1 (n=3) samples. Stress-strain curves between 0 – 40% of deformation of all 100 cycles for each sample are shown in Figure 3.7, Figure 3.8 and Figure 3.9, respectively.

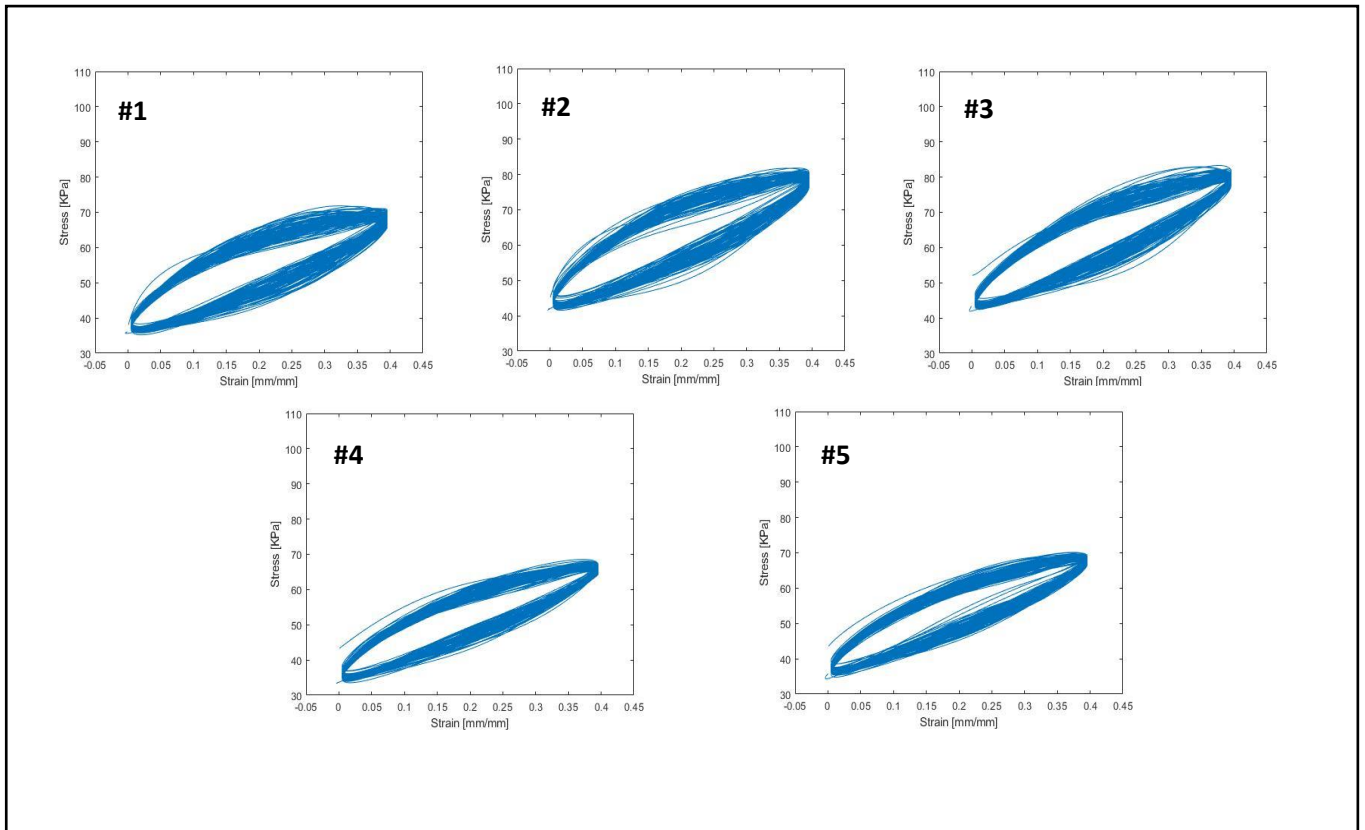


Figure 3.7: Stress-strain curves of RTV4524 (n=5) samples obtained from uniaxial cyclic tensile test.

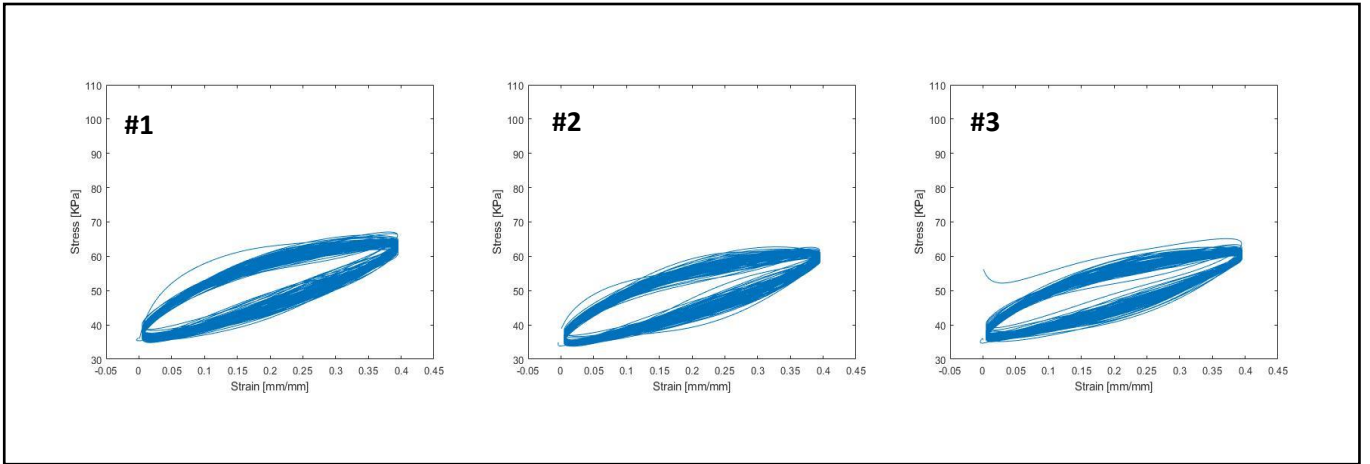


Figure 3.8: Stress-strain curves of R1.5/P1 ( $n=3$ ) samples obtained from uniaxial cyclic tensile test.

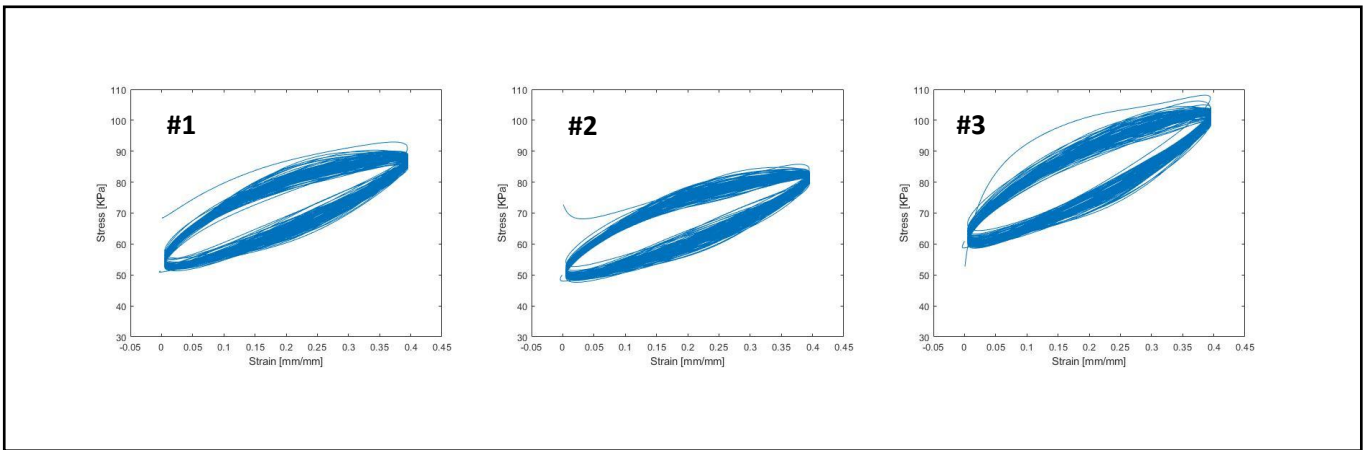


Figure 3.9: Stress-strain curves of R2/P1 ( $n=3$ ) samples obtained from uniaxial cyclic tensile test.

As it is possible to observe in the stress-strain curves showed above, all the materials show an elastic behaviour in the range of 0-40% strain, as each cycle is approximately superimposable to the other cycles.

For each sample, Young's modulus was evaluated by considering the slope of each load curve (0-40% deformation) and then averaged over the 100 cycles (Figure 3.10). The maximum stress at  $\epsilon=40\%$  was evaluated by taking into account the stress at  $\epsilon=40\%$  for every cycle and then averaged over the 100 cycles. The average results from each sample were then further averaged among similar samples and reported as mean  $\pm$  standard deviation (Figure 3.11).

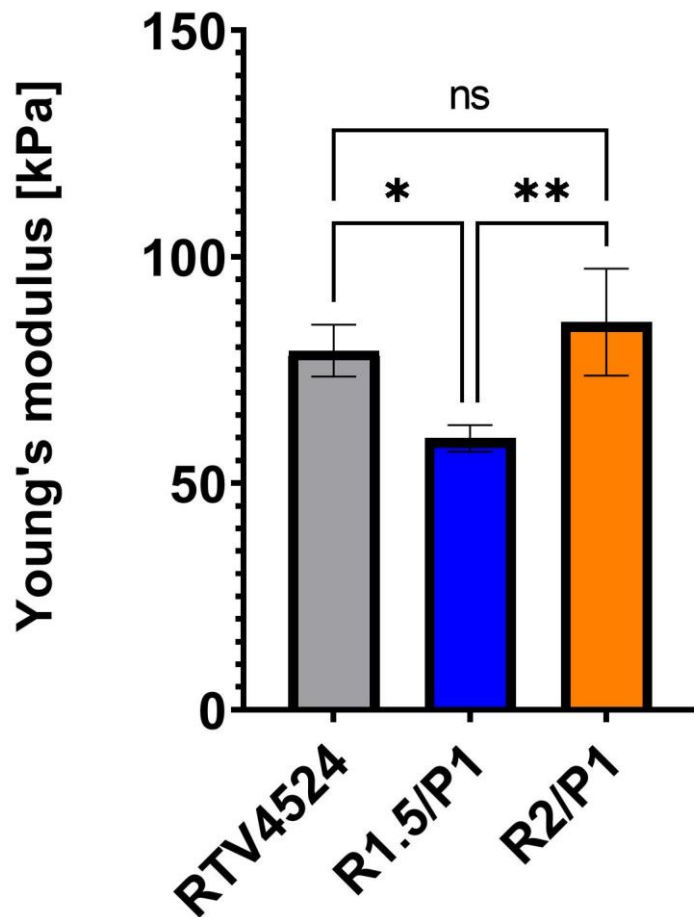


Figure 3.10: Average Young's modulus for RTV4524 (grey), R1.5/P1 (blue) and R2/P1 (orange) samples, obtained considering the deformation range from 0% to 40% strain.

The figure shows that the average Young's modulus is  $79.3 \pm 5.7$  KPa,  $59.9 \pm 2.9$  KPa and  $85.6 \pm 11.8$  KPa for RTV4524, R1.5/P1 and R2/P1, respectively. One-way ANOVA with Tukey's multiple comparisons test revealed that R1.5/P1 is significantly different from both RTV4524 and R2/P1 ( $P = 0.0162$  and  $P = 0.0065$ , respectively), while RTV4524 and R2/P1 are similar ( $P = 0.5021$ ).

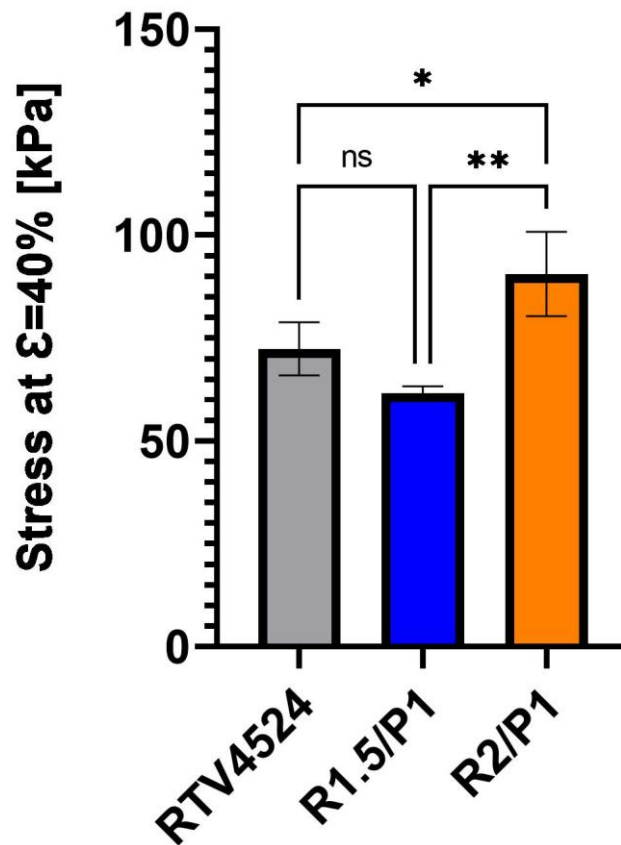


Figure 3.11: Average stress at  $\epsilon=40\%$  for RTV4524 (grey), R1.5/P1 (blue) and R2/P1 (orange) samples.

The results show that the average stress reached at  $\epsilon=40\%$  is  $72.4 \pm 6.4$  KPa,  $61.5 \pm 1.7$  KPa and  $90.5 \pm 10.2$  KPa for RTV4524, R1.5/P1 and R2/P1, respectively. One-way ANOVA with Tukey's multiple comparisons test revealed that R2/P1 is significantly different from both RTV4524 and R1.5/P1 ( $P = 0.0170$  and  $P = 0.0022$ , respectively), while RTV4524 and R2/P1 are similar ( $P = 0.1413$ ).

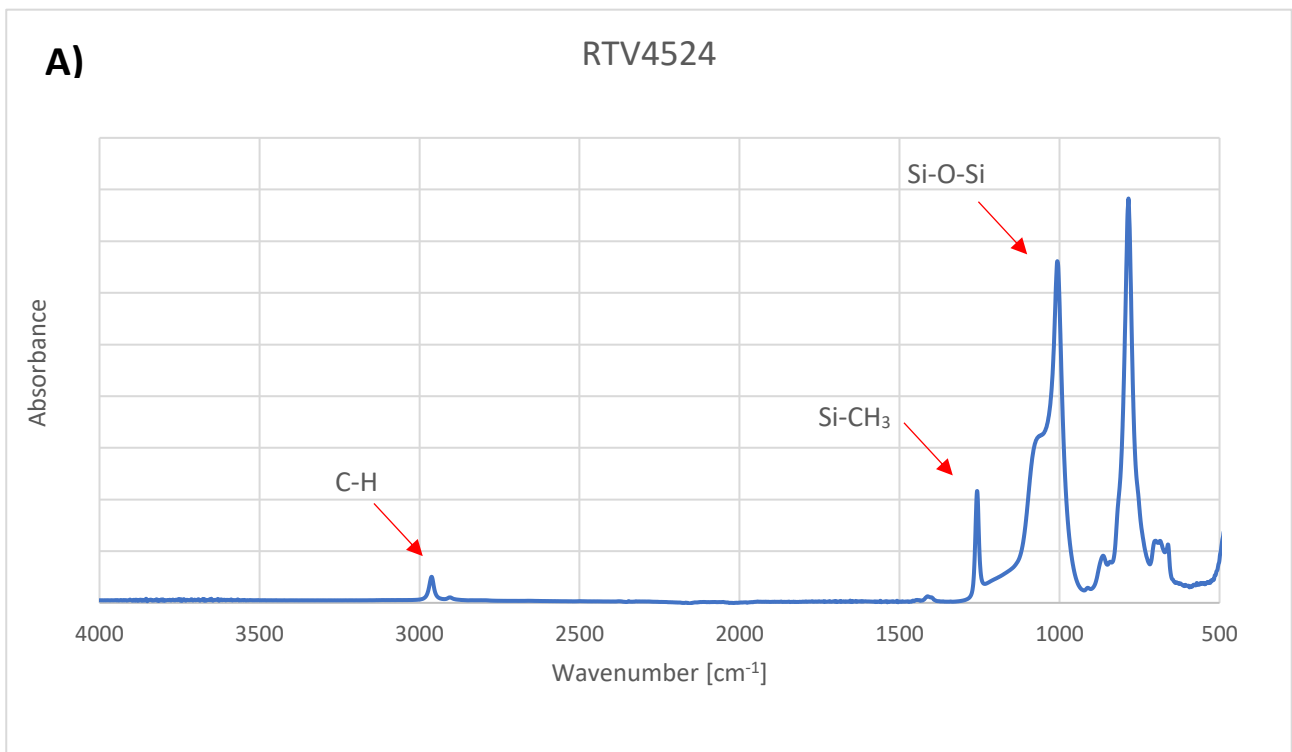
It is possible to state that R1.5/P1 appears more flexible than RTV4524, as its lower Young's modulus and stress at 40% strain implies it is easier to deform, while R2/P1 seems slightly stiffer than RTV4524. Furthermore, by comparing the two blends, it seems that the increase in the amount of silicone in the blend leads to an increase in mechanical properties: R2/P1 appears stiffer than R1.5/P1 and requires a higher load in order to be deformed up to 40% its original length. However, both blends showed a Young's modulus whose entity can be considered as comparable to that of natural vocal folds: A. Miri et al. report that Young's modulus of human tissue under tensile resistive

load and longitudinal stretch ranges around 50–200 kPa for the cover layer and 40–110 kPa for the body layer [42].

### 3.3 ATR-FTIR analysis

ATR-FTIR analysis was performed on RTV4524, R1.5/P1 and R2/P1 samples; the spectra are shown in

Figure 3.12.



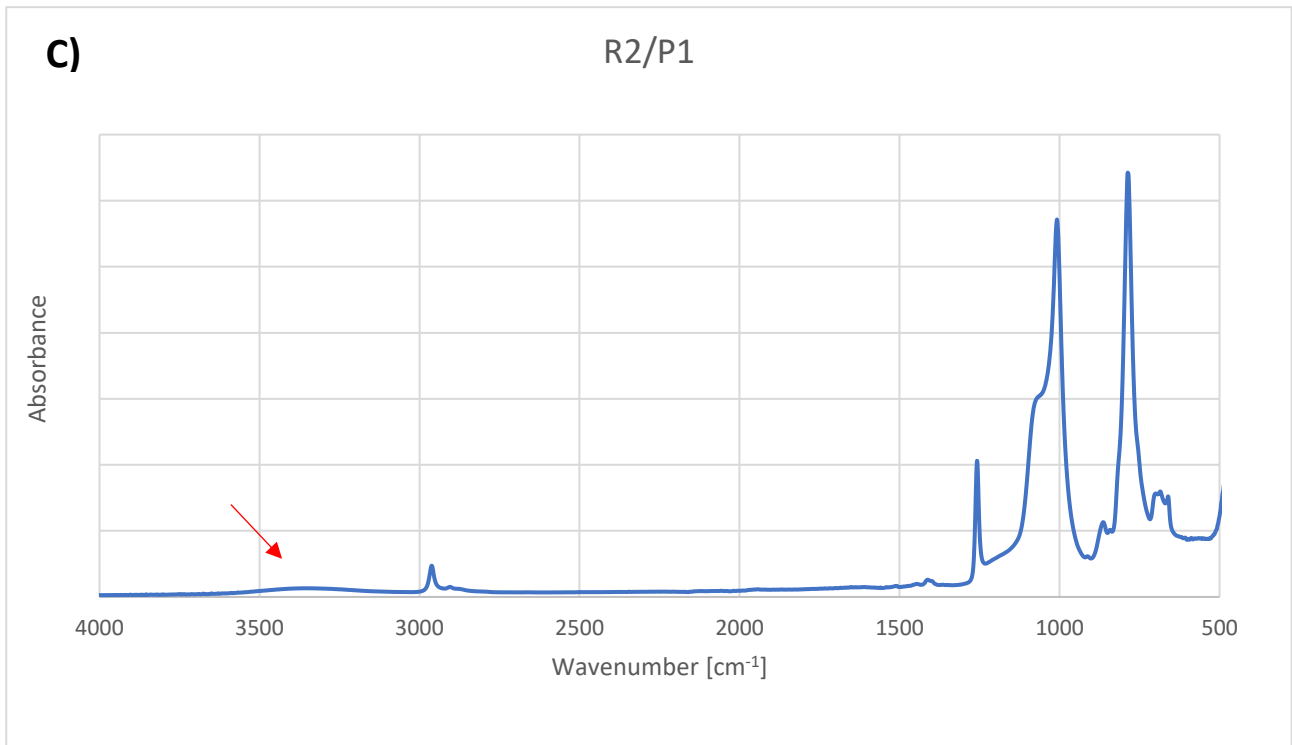
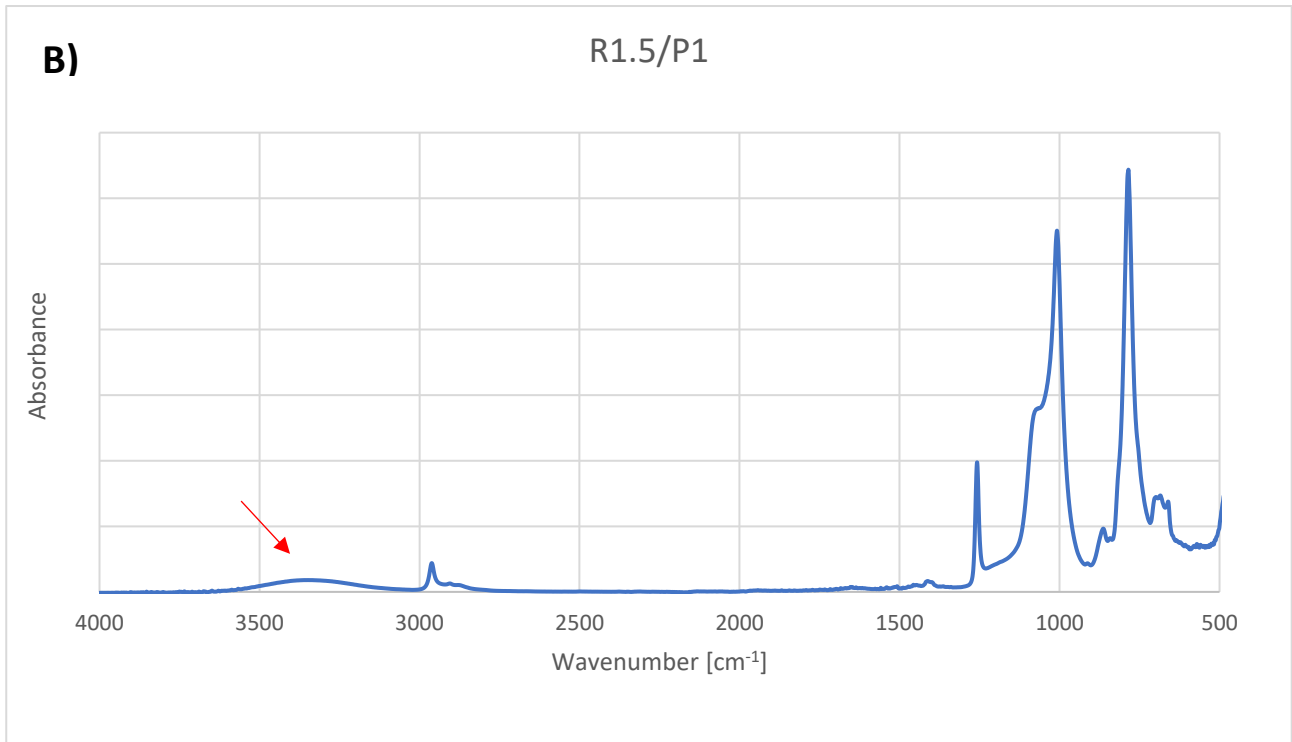


Figure 3.12: ATR-FTIR spectra of A) RTV4524, B) R1.5/P1 and C) R2/P1 and their characteristic peaks, indicated by red arrows.

Silicones show characteristic peaks at  $2960\text{ cm}^{-1}$  due to C–H bonds in  $\text{CH}_3$  groups, Si– $\text{CH}_3$  bonds (side chains) at  $1270\text{--}1255\text{ cm}^{-1}$  and Si–O–Si bonds (silicone backbones) at  $1100\text{--}1000\text{ cm}^{-1}$  [43]. According to literature, the FTIR spectrum of pristine PEDOT:PSS shows characteristic peaks at the stretching frequency of  $3700\text{ cm}^{-1}$  due to O–H stretching,  $3500\text{ cm}^{-1}$  due to C–H stretching,  $2900\text{ cm}^{-1}$  due to C=O and  $2500\text{ cm}^{-1}$  due to C–N stretching, a peak at  $1899\text{ cm}^{-1}$  is due to C=S bond stretching mode of the sulfoxide groups [44].

As it is possible to observe in

Figure 3.12 B) and C), the blends spectra show a peak at around  $3400\text{ cm}^{-1}$  that could be related to the presence of PEDOT:PSS' C-H bonds [44]. No other remarkable differences can be pointed out with respect to the RTV4524 spectrum.

### 3.4 WCA measurements

Wettability characterization was performed through WCA measurements. The results are illustrated in Figure 3.13 referred to RTV4524 and the blends, R1.5/P1 and R2/P1.

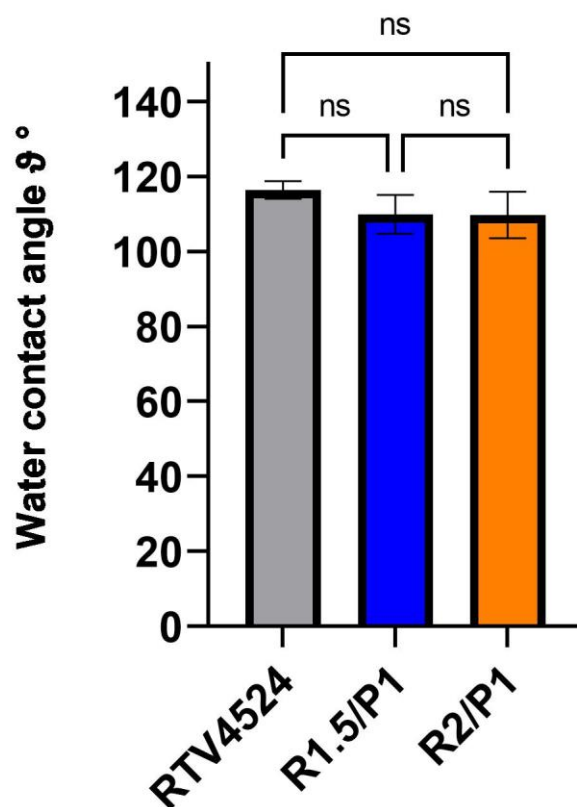


Figure 3.13: WCA measurements for RTV4524 (grey), R1.5/P1 (blue) and R2/P1 (orange) samples.

As it could be expected, RTV4524's surface shows a hydrophobic behaviour: the contact angle value is estimated around  $116.4^\circ \pm 2.4^\circ$ . Looking at the blends results, small differences can be pointed out: the addition of hydrophilic PEDOT:PSS, yielding an interconnected network of RTV4524 and PEDOT:PSS slightly decreases the hydrophobicity of the surface: the contact angle evaluated is around  $109.8^\circ \pm 5.2^\circ$  and  $109.7^\circ \pm 6.2^\circ$  for R1.5/P1 and R2/P1, respectively. One-way ANOVA with Tukey's multiple comparisons test revealed that all the three materials were similar to each other ( $P = 0.2984$  for RTV4524 vs. R1.5/P1,  $P = 0.2865$  for RTV4524 vs. R2/P1,  $P = 0.9994$  for R1.5/P1 vs. R2/P1). It can be stated that, in terms of surface wettability, the silicone, hydrophobic part of the blend, has a higher impact than PEDOT:PSS, the hydrophilic one. The results are in line with the ATR-FTIR analysis, where only a small peak relating to the presence of PEDOT:PSS in the surface was detected in both blends' spectra.

### 3.5 Indirect cytotoxicity test

An indirect cytotoxicity test was carried out following the protocol described in section 2.6. In Figure 3.14 and Figure 3.15 the resorufin fluorescence derived from the fibroblasts' cultures ( $1 \times 10^4$  and  $2 \times 10^4$  cells/well, respectively) exposed to RTV4524, R1.5/P1 and R2/P1 conditioned mediums after 24-48-72h is shown; the control (CTRL) is represented by the signal emitted by a cellular culture using not-conditioned medium. Three samples for each type of medium were tested, the results have been reported as mean  $\pm$  standard deviation. Figure 3.16 and Figure 3.17 shows the resorufin fluorescence expressed as a percentage of the CTRL fluorescence, reported as mean  $\pm$  standard deviation. Two-ways ANOVA with Tukey's multiple comparisons test has been made between the four different mediums for every time point. In every figure are shown the comparisons where a statistically significant difference was detected, every other comparison result not shown is intended to be not significant ( $P > 0.05$ ).

Resorufin fluorescence was used as an indicator of cells viability for 10.000 cells/well and 20.000 cells/well densities exposed to media conditioned by R1.5/P1 (blue), R2/P1 (orange), or RTV4524 (grey) versus cells cultured with a not-conditioned medium, used as a control (green). Results are reported as mean  $\pm$  standard deviation averaged from  $n=3$  samples.

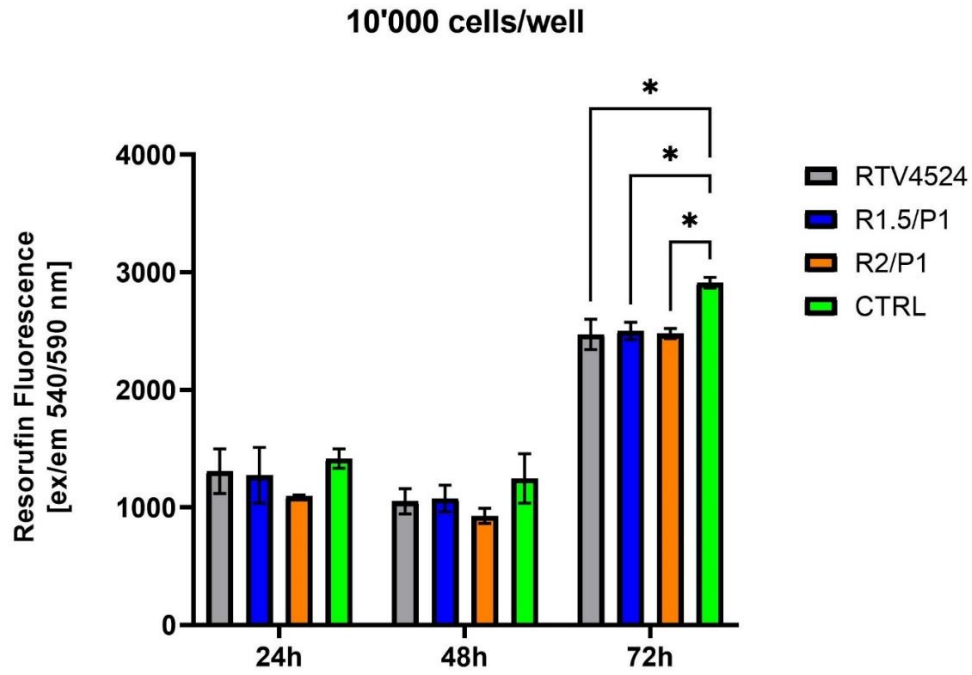


Figure 3.14: Resorufin fluorescence as an indicator of cells viability for cells ( $1 \times 10^4$  cells/well) exposed to different conditioned media. Results are reported as mean  $\pm$  standard deviation averaged from  $n=3$  samples.

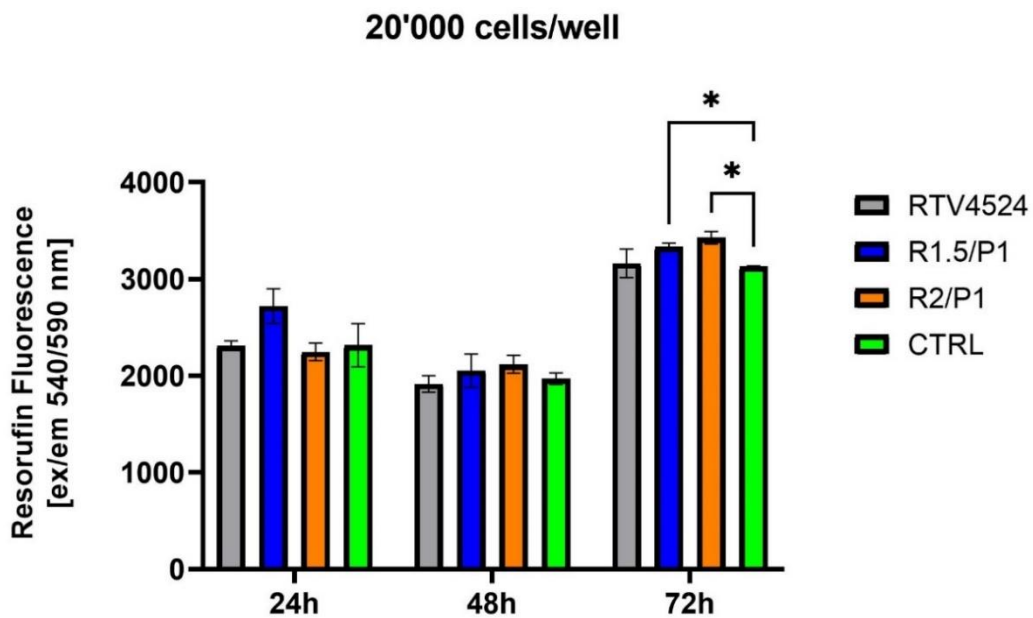


Figure 3.15: Resorufin fluorescence as an indicator of cells viability for cells ( $2 \times 10^4$  cells/well) exposed to different conditioned media. Results are reported as mean  $\pm$  standard deviation averaged from  $n=3$  samples.

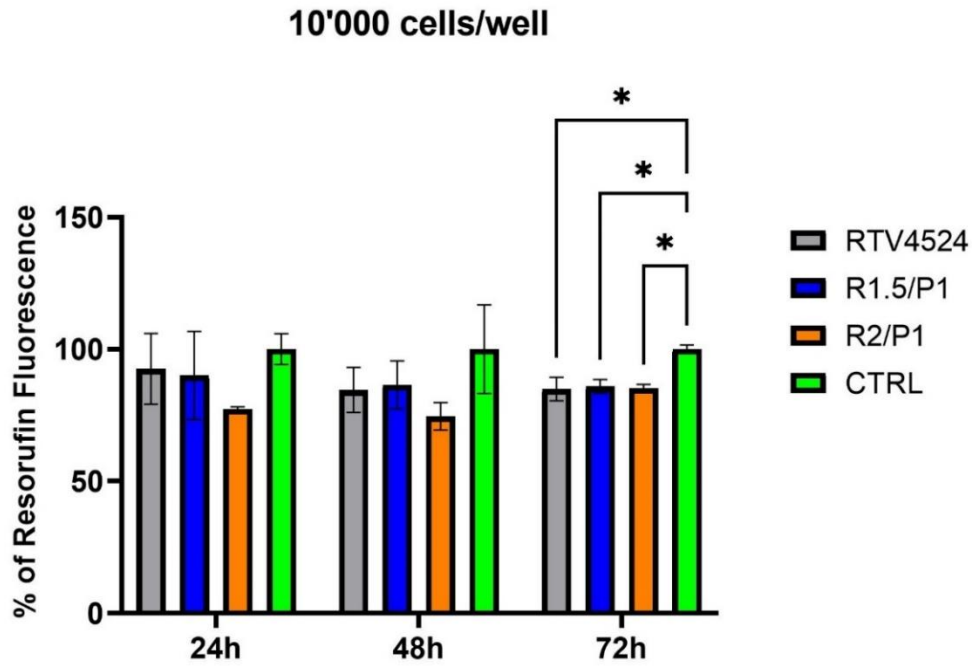


Figure 3.16: Percentage of resorufin fluorescence as an indicator of cells viability for cells ( $1 \times 10^4$  cells/well) exposed to different conditioned media, with respect to the control (CTRL). Results are reported as mean  $\pm$  standard deviation averaged from  $n=3$  samples.

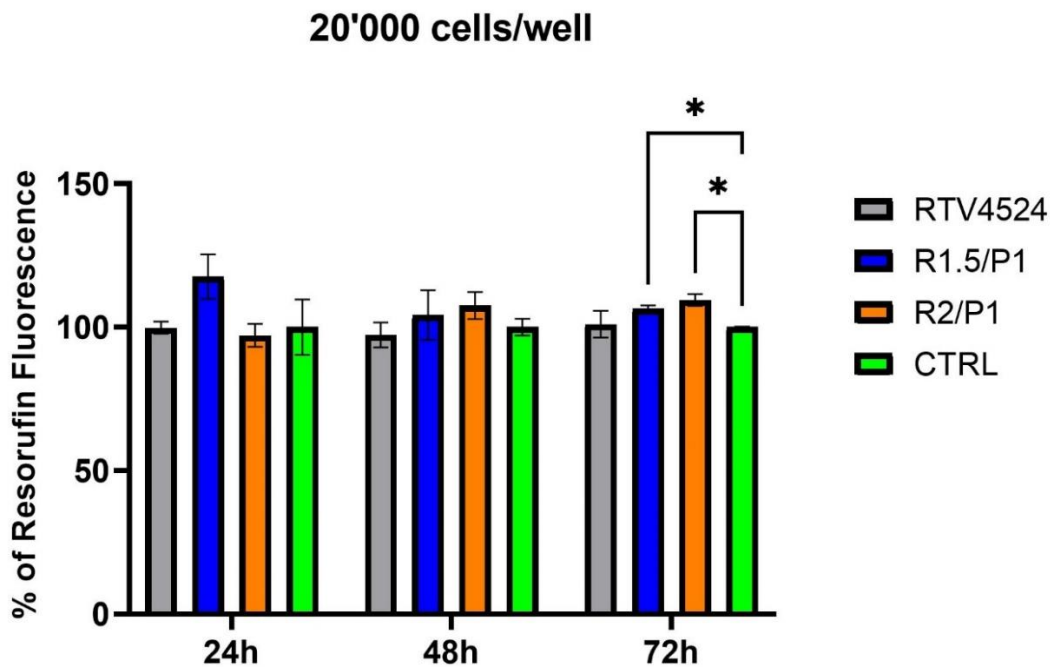


Figure 3.17: Percentage of resorufin fluorescence as an indicator of cells viability for cells ( $2 \times 10^4$  cells/well) exposed to different conditioned media, with respect to the control (CTRL). Results are reported as mean  $\pm$  standard deviation averaged from  $n=3$  samples.

Looking at the results, in both  $1 \times 10^4$  and  $2 \times 10^4$  cells population it is possible to notice a small decrease in fluorescence from the 24h to the 48h time point in every type of medium tested. However, at 72h viability increases again, rejecting the hypothesis of a potential cytotoxic behaviour.

By comparing the two different cells densities, in  $1 \times 10^4$  cells it can be observed that both the media conditioned with the blends seem to show a similar fluorescence than the medium conditioned with pure RTV4524 at every time point, while, with respect to the control, there is a statistically significant difference in the last time point at 72h only; however, the percentage of resorufin fluorescence for both blends at that timepoint is at least 85% of the control value.

A similar behaviour can be observed for  $2 \times 10^4$  cells/well: both media conditioned with R1.5/P1 or R2/P1 blend manifest a similar fluorescence values than those relative to RTV4524 at every time point, and, with respect to the control, there is a statistically significant difference in the last time point at 72h only. Thus, the 72h timepoint for both cells densities does not display any considerable differences among the three conditioned media tested and, with respect to the control, the fluorescence value is at least 85% for  $1 \times 10^4$  cells/well and 101% for  $2 \times 10^4$  cells/well: neither RTV4524, R1.5/P1 nor R2/P1 show a cytotoxic effect against the cells.

## 4 Conclusions

PEDOT:PSS, a hydrophilic conductive polymer, was chosen to blend with a hydrophobic silicone elastomer, as an alternative strategy with respect to the more traditional one based on adding conductive nanofillers (such as metallic nanoparticles and carbon nanotubes) in an elastomeric matrix, in order to obtain a conductive elastomer: a material with enhanced electrical conductivity that also showed good stretchability and biocompatibility properties. The first part of the work concerned the optimization of the blending protocol: at first, PDMS was chosen for its known properties of biocompatibility and versatility. Multiple attempts were conducted to obtain an homogenous PDMS-PEDOT:PSS blend, with the addition of Triton X-100 as surfactant and Ethylene Glycol as dopant, but none of them was successful. Non-homogeneity and phase separation observed between the two polymers could have been caused by the relatively elevated time PDMS needs to cure (48 hours at least). Therefore, PDMS was replaced with Silbione RTV4524 (RTV4524), another silicone elastomer capable of curing in a much shorter time (around 45 minutes). Different blends were prepared by mixing this elastomer with PEDOT:PSS, varying the silicone/conductive polymer ratio but maintaining constant the percentages of Triton X-100 and Ethylene Glycol in relation to the quantity of PEDOT:PSS at 1% v/v and 7% v/v, respectively. Results appeared more promising since homogeneity was achieved for every formulation tested. After the optimization phase, two different formulations of the blend (2/1 and 1.5/1 ratios) were chosen and subjected to various material characterization tests. Surface characterizations such as ATR-FTIR analysis revealed the presence of PEDOT:PSS absorption bands in the surface, despite Water Contact Angle measurements showed that the silicone was predominant with respect to PEDOT:PSS, as the blends manifested a hydrophobic behaviour very similar to pristine RTV4524. Preliminary results from uniaxial tensile testing at break revealed that blending RTV4524 with PEDOT:PSS led to a decrease in mechanical properties compared to pristine silicone elastomer, although being suitable for the specific application. Further mechanical testing showed that both formulations were capable of cyclic elastic deformation up to 40% of their original length without showing any evident damage or decrease in performances and had Young's moduli comparable to that of natural vocal folds. Indirect cytotoxicity test through resazurin assay revealed that none of the two formulations showed a behaviour that could be interpreted as harmful to cells. Electrical conductivity of the blends is

currently under investigation: electromechanical tests are being conducted in order to evaluate if the blends show an appropriate conductivity that would make them suitable for being integrated and properly tested with a voice/larynx prosthetic device.

For what concerns future developments, further biological characterizations, such as interactions with bacteria, should be performed to fully validate a potential *in vivo* application: silicones are known for occasionally being problematic in terms of bacterial adhesion and biofilm formation when considering long term implants, therefore a silicone-based material is likely to show the same issues. In such a case, the biomaterial could be subjected to surface functionalization, grafting specific molecules (such as antimicrobial and antifouling biomolecules) that could provide or enhance useful features for the specific application.

## 5 Bibliography

- [1] Noordzij, J.P. and Ossoff, R.H. (2006) Anatomy and physiology of the larynx. *Otolaryngologic Clinics of North America*, **39**, 1–10. <https://doi.org/10.1016/j.otc.2005.10.004>
- [2] Pereira, O., Malysz, T., Jotz, G.P. and Ant, M. (2014) A Morphometric Study of the Larynx. *Journal of Voice*, 1–5. <https://doi.org/10.1016/j.jvoice.2014.03.008>
- [3] HIRANO, M., KAKITA, Y., OHMARU, K. and KURITA, S. (1982) Structure and Mechanical Properties of the Vocal Fold [Internet]. Speech and Language. ACADEMIC PRESS, INC. <https://doi.org/10.1016/b978-0-12-608607-2.50015-7>
- [4] Hahn, M.S., Kobler, J.B., Zeitels, S.M. and Langer, R. (2006) Quantitative and comparative studies of the vocal fold extracellular matrix I: Collagen. *Annals of Otology, Rhinology and Laryngology*, **115**, 156–64. <https://doi.org/10.1177/000348940611500213>
- [5] Hahn, M.S., Kobler, J.B., Zeitels, S.M. and Langer, R. (2006) Quantitative and comparative studies of the vocal fold extracellular matrix II: Collagen. *Annals of Otology, Rhinology and Laryngology*, **115**, 225–32. <https://doi.org/10.1177/000348940611500311>
- [6] Alipour, F. and Jaiswal, S. (2008) Phonatory characteristics of excised pig, sheep, and cow larynges. *The Journal of the Acoustical Society of America*, **123**, 4572–81. <https://doi.org/10.1121/1.2908289>
- [7] Alipour, F. and Jaiswal, S. (2009) Glottal Airflow Resistance in Excised Pig, Sheep, and Cow Larynges. *Journal of Voice*, The Voice Foundation. **23**, 40–50. <https://doi.org/10.1016/j.jvoice.2007.03.007>
- [8] Thomson, S.L., Mongeau, L. and Frankel, S.H. (2005) Aerodynamic transfer of energy to the vocal folds. *The Journal of the Acoustical Society of America*, **118**, 1689–700. <https://doi.org/10.1121/1.2000787>
- [9] Murray, P.R. and Thomson, S.L. (2011) Synthetic, multi-layer, self-oscillating vocal fold model fabrication. *Journal of Visualized Experiments*, 2–7. <https://doi.org/10.3791/3498>
- [10] Slavitt, D.H., Lipton, R.J. and Mccaffrey, T. V. (1990) Glottographic analysis of phonation in

the excised canine larynx. *Annals of Otology, Rhinology & Laryngology*, **99**, 396–402.  
<https://doi.org/10.1177/000348949009900514>

- [11] Verdolini, K., Chan, R., Titze, I.R., Hess, M. and Bierhals, W. (1998) Correspondence of electroglottographic closed quotient to vocal fold impact stress in excised canine larynges. *Journal of Voice*, **12**, 415–23. [https://doi.org/10.1016/S0892-1997\(98\)80050-7](https://doi.org/10.1016/S0892-1997(98)80050-7)
- [12] Scherer, R.C., Titze, I.R. and Curtis, J.F. (1983) Pressure-flow relationships in two models of the larynx having rectangular glottal shapes. **73**, 668–76.
- [13] Zhang, Z., Neubauer, J. and Berry, D.A. (2006) Aerodynamically and acoustically driven modes of vibration in a physical model of the vocal folds. *The Journal of the Acoustical Society of America*, **120**, 2841–9. <https://doi.org/10.1121/1.2354025>
- [14] Zhang, Z., Neubauer, J. and Berry, D.A. (2006) The influence of subglottal acoustics on laboratory models of phonation. *The Journal of the Acoustical Society of America*, **120**, 1558–69. <https://doi.org/10.1121/1.2225682>
- [15] Shaw, S.M., Thomson, S.L., Dromey, C. and Smith, S. (2012) Frequency Response of synthetic vocal fold models. *Journal of Speech, Language, and Hearing Research*, **55**, 1396–406. [https://doi.org/10.1044/1092-4388\(2012/11-0153\)a](https://doi.org/10.1044/1092-4388(2012/11-0153)a)
- [16] Baken, R.J. (1992) Electroglottography. *Journal of Voice*, **6**, 98–110.  
[https://doi.org/10.1016/S0892-1997\(05\)80123-7](https://doi.org/10.1016/S0892-1997(05)80123-7)
- [17] Syndergaard, K.L., Dushku, S. and Thomson, S.L. (2017) Electrically conductive synthetic vocal fold replicas for voice production research. *The Journal of the Acoustical Society of America*, **142**, EL63–8. <https://doi.org/10.1121/1.4990540>
- [18] Leonhard, M. and Schneider-Stickler, B. (2015) Voice prostheses, microbial colonization and biofilm formation. *Advances in Experimental Medicine and Biology*, **830**, 123–36.  
[https://doi.org/10.1007/978-3-319-11038-7\\_8](https://doi.org/10.1007/978-3-319-11038-7_8)
- [19] Palza, H., Zapata, P.A. and Angulo-pineda, C. (2019) Electroactive Smart Polymers for Biomedical Applications. *Materials*,. <https://doi.org/10.3390/ma12020277>
- [20] Balint, R., Cassidy, N.J. and Cartmell, S.H. (2014) Conductive polymers: Towards a smart

biomaterial for tissue engineering. *Acta Biomaterialia*, Acta Materialia Inc. **10**, 2341–53.  
<https://doi.org/10.1016/j.actbio.2014.02.015>

- [21] Street, J.L.B.G.B. (1985) Polarons , Bipolarons , and Solitons in Conducting Polymers. 309–15. <https://doi.org/10.1021/ar00118a005>
- [22] Jouni, M., Djurado, D., Massardier, V. and Boiteux, G. A Representative and Comprehensive Review on the Electrical and Thermal Properties of Polymer Composites with Carbon Nanotube and other Nanoparticle Fillers.
- [23] Alamusi, Hu, N., Fukunaga, H., Atobe, S., Liu, Y. and Li, J. (2011) Piezoresistive strain sensors made from carbon nanotubes based polymer nanocomposites. *Sensors*, **11**, 10691–723.  
<https://doi.org/10.3390/s111110691>
- [24] Liu, H., Li, Q., Zhang, S., Yin, R., Liu, X. and He, Y. (2018) Electrically conductive polymer composites for smart flexible strain sensors : a critical review. Royal Society of Chemistry. 12121–41. <https://doi.org/10.1039/c8tc04079f>
- [25] Caló, E. and Khutoryanskiy, V. V. (2015) Biomedical applications of hydrogels: A review of patents and commercial products. *European Polymer Journal*, **65**, 252–67.  
<https://doi.org/10.1016/j.eurpolymj.2014.11.024>
- [26] Lenick, A.J.O. (2000) Silicones — Basic Chemistry and Selected Applications. *Journal of Surfactants and Detergents*, **3**, 229–36.
- [27] Shit, S.C. and Shah, P. (2013) A Review on Silicone Rubber. *The National Academy of Sciences*, **36**, 355–65. <https://doi.org/10.1007/s40009-013-0150-2>
- [28] Ylgör, E. and Ylgör, I. (2001) Hydrogen bonding: A critical parameter in designing silicone copolymers. *Polymer*, **42**, 7953–9. [https://doi.org/10.1016/S0032-3861\(01\)00293-2](https://doi.org/10.1016/S0032-3861(01)00293-2)
- [29] Vaicekauskaite, J., Mazurek, P., Vudayagiri, S. and Skov, A.L. (2020) Mapping the mechanical and electrical properties of commercial silicone elastomer formulations for stretchable transducers. *Journal of Materials Chemistry C*, Royal Society of Chemistry. **8**, 1273–9.  
<https://doi.org/10.1039/c9tc05072h>
- [30] Mazurek, P. (2019) How to tailor flexible silicone elastomers with mechanical integrity : a

tutorial review. *Chemical Society Reviews*, Royal Society of Chemistry.

<https://doi.org/10.1039/c8cs00963e>

- [31] Kalman, P.G., Ward, C.A., McKeown, N.B., McCullough, D. and Romaschin, A.D. (1991) Improved biocompatibility of silicone rubber by removal of surface entrapped air nuclei. *Journal of Biomedical Materials Research*, **25**, 199–211.  
<https://doi.org/10.1002/jbm.820250207>
- [32] Williams, D.F. (2008) On the mechanisms of biocompatibility. *Biomaterials*, **29**, 2941–53.  
<https://doi.org/10.1016/j.biomaterials.2008.04.023>
- [33] Abbasi, F., Mirzadeh, H. and Katbab, A. (2001) Modification of polysiloxane polymers for biomedical applications : a review. *Polymer International*, **1287**.  
<https://doi.org/10.1002/pi.783>
- [34] Gottenbos, B., Van Der Mei, H.C., Klatter, F., Nieuwenhuis, P. and Busscher, H.J. (2002) In vitro and in vivo antimicrobial activity of covalently coupled quaternary ammonium silane coatings on silicone rubber. *Biomaterials*, **23**, 1417–23. [https://doi.org/10.1016/S0142-9612\(01\)00263-0](https://doi.org/10.1016/S0142-9612(01)00263-0)
- [35] A. Ibrahim, B. and M.Kadum, K. (2010) Influence of Polymer Blending on Mechanical and Thermal Properties. *Modern Applied Science*, **4**, 157–61.  
<https://doi.org/10.5539/mas.v4n9p157>
- [36] Anna Hillerstrom, B.K. (2008) A Two-Step Method for the Synthesis of a Hydrophilic PDMS Interpenetrating Polymer Network. *Journal of Applied Polymer Science*, **110**, 3059–67.  
<https://doi.org/10.1002/app>
- [37] Wang, Y. (2009) Research progress on a novel conductive polymer-poly(3,4-ethylenedioxythiophene) (PEDOT). *Journal of Physics: Conference Series*, **152**.  
<https://doi.org/10.1088/1742-6596/152/1/012023>
- [38] Kayser, L. V. and Lipomi, D.J. (2019) Stretchable Conductive Polymers and Composites Based on PEDOT and PEDOT:PSS. *Advanced Materials*, **31**, 1–13.  
<https://doi.org/10.1002/adma.201806133>
- [39] Shi, H., Liu, C., Jiang, Q. and Xu, J. (2015) Effective Approaches to Improve the Electrical

Conductivity of PEDOT:PSS: A Review. *Advanced Electronic Materials*, **1**, 1–16.

<https://doi.org/10.1002/aelm.201500017>

- [40] Luo, R., Li, H., Du, B., Zhou, S. and Zhu, Y. (2020) A simple strategy for high stretchable, flexible and conductive polymer films based on PEDOT:PSS-PDMS blends. *Organic Electronics*, Elsevier. **76**, 105451. <https://doi.org/10.1016/j.orgel.2019.105451>
- [41] Hsiao, T.Y., Wang, C.L., Chen, C.N., Hsieh, F.J. and Shau, Y.W. (2002) Elasticity of human vocal folds measured in vivo using color Doppler imaging. *Ultrasound in Medicine and Biology*, **28**, 1145–52. [https://doi.org/10.1016/S0301-5629\(02\)00559-8](https://doi.org/10.1016/S0301-5629(02)00559-8)
- [42] Miri, A.K. (2014) Mechanical characterization of vocal fold tissue: A review study. *Journal of Voice*, Elsevier Ltd. **28**, 657–67. <https://doi.org/10.1016/j.jvoice.2014.03.001>
- [43] Zhu, Y., Otsubo, M., Honda, C. and Tanaka, S. (2006) Loss and recovery in hydrophobicity of silicone rubber exposed to corona discharge. *Polymer Degradation and Stability*, **91**, 1448–54. <https://doi.org/10.1016/j.polyimdegradstab.2005.10.014>
- [44] Pasha, A., Roy, A.S., Murugendrappa, M. V., Al-Hartomy, O.A. and Khasim, S. (2016) Conductivity and dielectric properties of PEDOT-PSS doped DMSO nano composite thin films. *Journal of Materials Science: Materials in Electronics*, Springer US. **27**, 8332–9. <https://doi.org/10.1007/s10854-016-4842-5>